Supplement of Nat. Hazards Earth Syst. Sci., 24, 2773–2791, 2024
https://doi.org/10.5194/nhess-24-2773-2024-supplement

Natural Hazards and Earth System Sciences
Open Access
EGU

Supplement of

Modelling tsunami initial conditions due to rapid coseismic seafloor displacement: efficient numerical integration and a tool to build unit source databases

Alice Abbate et al.

Correspondence to: Alice Abbate (alice.abbate@ingv.it)

S1 Unit tsunamigenic source: numerical solution in one dimension

S1.1 Calculations for assessing the convergence of the model

In one dimension, the free surface perturbation reduces to (Nosov and Sementsov 2014):

$$\xi_0(x) = \frac{2B_0}{\pi} \int_0^\infty \frac{\cos(mx)\sin(ma)}{m\cosh(mH_0)} dm \tag{1}$$

being B_0 the amplitude of the bottom deformation and H_0 the sea-depth, both assumed to be constant along a. The variable of integration m represents the spatial wavenumber and quantifies the number of oscillations of the integrand function along a. To numerically solve the integral, we follow these steps:

1. Evaluate the convergence of the integral by:
   (a) Dealing with the singularity at $m = 0$;
   (b) Proving that it exists a value U such that the primitive of the integral contributes negligibly for all wave numbers $m \gg U$.

We split Eq. (1) into the sum of three terms:

$$\xi_0(x) = \frac{2B_0}{\pi} \left(\int_0^\epsilon \frac{\cos(mx)\sin(ma)}{m\cosh(mH_0)} dm + \int_\epsilon^U \frac{\cos(mx)\sin(ma)}{m\cosh(mH_0)} dm + \int_U^\infty \frac{\cos(mx)\sin(ma)}{m\cosh(mH_0)} dm \right) \tag{2}$$

with $\epsilon \ll 1$. We consider the first term in Eq. (2) and we use the Taylor expansions to the third order of $\frac{\sin(ma)}{m}$ and $\cos(mx)$, respectively. It follows that:

$$\begin{aligned} \frac{\sin(ma)}{m} &= a + O(m^2) \\ \cos(mx) &= 1 + O(m^2) \end{aligned} \tag{3}$$

Since $\lim_{m\to 0} \cosh(mH_0) = 1$ and $cosh(mH_0) > 1 \quad \forall m, H_0 \in \mathbf{R}$:

$$\int_0^\epsilon \frac{\cos(mx)\sin(ma)}{m\cosh(mH_0)} dm \simeq \int_0^\epsilon (a + O(m^2))(1 + O(m^2)) dm = a\epsilon + O(\epsilon^3) \tag{4}$$

meaning that the singularity at $m = 0$ is negligible. In particular, the truncation error $O(\epsilon^3)$ ensures that the first term in Eq. (2) is upper bounded by ϵ^3. We then consider the third term in Eq. (2). We take advantage of the triangular inequality and of the fact that both sine and cosine are bounded by one in absolute value. Reminding that the hyperbolic cosine $\cosh(mH) = \frac{e^{mH} + e^{-mH}}{2}$ is always greater than one and in particular defined positive $\forall m \in \mathbf{R}$, the following considerations can be done:

$$\left| \int_U^\infty \frac{\cos(mx)\sin(ma)}{m\cosh(mH_0)} dm \right| \leq \int_U^\infty \left| \frac{\cos(mx)\sin(ma)}{m\cosh(mH_0)} \right| dm \leq \tag{5}$$

$$\leq \int_U^\infty \frac{1}{m\cosh(mH_0)} dm = \int_U^\infty \frac{2}{m(e^{mH_0} + e^{-mH_0})} dm = \tag{6}$$

$$= \int_U^\infty \frac{2}{me^{mH_0}(1 + e^{-2mH_0})} dm \leq 2 \int_U^\infty m^{-1} e^{-mH_0} dm \tag{7}$$

because the term $1 + e^{-2mH_0}$ at the denominator is grater than one $\forall m, H_0 \in \mathbf{R}$. It would be helpful to perform a change of variables. We will call $t = mH_0$ from which $dt = dmH_0$. Plugging this substitutions into (5), we will obtain:

$$2 \int_{UH_0}^\infty m^{-1} e^{-mH_0} dm = 2 \int_{UH_0}^\infty t^{-1} e^{-t} dt$$

We observe that this integral has the same shape of the *gamma function*:

$$\Gamma(x)_{|_{x=0}} = \int_0^\infty t^{x-1} e^{-t} dt$$

Since we are seeking for convergence only in an integral support ranging in $[U, \infty)$, we can bound the integral underlying that for very large t the exponential function $e^{-\frac{t}{2}}$ decays much faster than t^{-1}. This is particularly true if $t \gg 1$, which implies that $mH_0 \gg 1 \quad \forall m \in \mathbf{R}$. Physically speaking, the latter condition refers to wavelengths much smaller than the depth, i.e. λ_0, which is the filtering condition of Kajiura (1963). As a consequence:

$$2 \int_{UH_0}^\infty t^{-1} e^{-t} dt \leq 2 \int_{UH_0}^\infty e^{-t} e^{\frac{t}{2}} dt = 2 \int_{UH_0}^\infty e^{-\frac{t}{2}} dt$$

Going back to the integration with respect to the variable m, this is equivalent to:

$$2 \int_U^\infty H_0 e^{-\frac{mH_0}{2}} dm = 4 \int_U^\infty -\frac{H_0}{2} e^{-\frac{mH_0}{2}} dm$$

Finally, we obtain:

$$\left| \int_U^\infty \frac{\cos(mx)\sin(ma)}{m\cosh(mH_0)} dm \right| \leq 4 \int_U^\infty -\frac{H_0}{2} e^{-\frac{mH_0}{2}} dm = \left[-4e^{-\frac{mH_0}{2}} \right]_U^\infty = 4e^{-\frac{UH_0}{2}}$$

which is a finite quantity. Thus, Eq. (1) converges and can be restated as a sum of a proper integral plus an infinitesimal error that approaches zero as $U \gg \frac{2}{H_0}$. The magnitude of the error depends on the product between the upper bound U used to truncate the support of integral and the depth value H_0 This suggests us that we can define a specific value for U depending on the precision we would achieve in performing numerical integration.

Considering U as a wavenumber that defines the upper boundary of the integral support, we can restate Eq. (1) as:

$$\xi_0(x) = \frac{2B_0}{\pi}\left(a\epsilon + O(\epsilon^3) + \int_{\epsilon}^{U} \frac{\cos(mx)\sin(ma)}{m\cosh(mH_0)}dm + o(e^{-\frac{UH_0}{2}})\right) \tag{8}$$

The term $o(e^{-\frac{UH_0}{2}})$ ensures that the third term in Eq. (2) is negligible, as it decreases faster than $e^{-\frac{UH_0}{2}}$.

Convergence is guaranteed when $\epsilon \ll 1$ and $U \gg \frac{2}{H_0}$, being H_0 the water depth, meaning that wavelengths $\lambda \ll \frac{H_0}{2}$ do not contribute to the tsunami generation model.

S1.1.1 Corner wavenumber for truncation

Figure S1 shows the case where the cell size a, the sea depth H_0 and the sea floor deformation B_0 are kept constant, while the upper limit for the integral support varies from $U = \frac{0.5}{H_0}$ to $U = \frac{5}{H_0}$.

For $U \leq \frac{2}{H_0}$, the peak of the truncated numerical solution is half of the reference solution, generally failing to accurately reconstruct the reference sea-surface profile. However, increasing the upper limit for the integral support to $U > \frac{2}{H_0}$ results in a good approximation of the initial sea-surface perturbation, though it introduces highly oscillating tails due to the limited number of wavenumbers considered. When the upper limit is set to $U = \frac{5}{H_0}$, the solution is stable.

S1.2 Optimal quadrature method for numerically solving the integral

Since both sine and cosine cannot be greater than one, equation (8) can be re-stated in a more convenient scaled version:

$$\xi_0(x_p) \simeq U\frac{2B_0}{\pi}\left(\frac{a\epsilon}{U} + \int_{m=\frac{\epsilon}{U}}^{1} \frac{\cos(mUx_p)\sin(mUa)}{mU\cosh(mUH_0)}dm\right) \tag{9}$$

and solved at each point x_p in the LED

$$l_e = \left(-4H_0 - \frac{a}{2},\ 4H_0 + \frac{a}{2}\right) \tag{10}$$

associated to the cell. In Section 2 of the main text, we set $U = \frac{5}{H_0}$ and $\epsilon = 10^{-9}$.

The support of the integral $\left[\frac{\epsilon}{U}, 1\right]$ in Eq. (9) is partitioned into a family of sub-intervals:

$$\left\{\left[\frac{\epsilon}{U}, \frac{\epsilon}{U} + dm\right], \left[\frac{\epsilon}{U} + dm, \frac{\epsilon}{U} + 2dm\right], \ldots, \left[1 - dm, 1\right]\right\} \tag{11}$$

where:

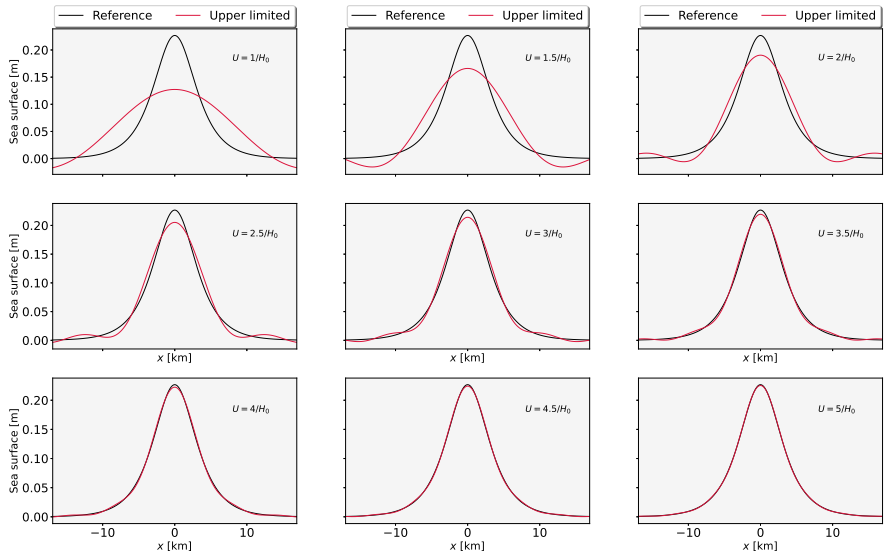

Figure S1. The cell size is kept constant to $a = 30$ arc-sec. The sea-depth is $H_0 = 4$ km and the amplitude of the sea bottom deformation is $B_0 = 1$ for all the cases.

$$dm = \frac{1 - \frac{\epsilon}{U}}{N_m}$$

and N_m is the number of sub-intervals as given by:

$$N_m = \max\left[2w_{max}, N_s\right] \tag{12}$$

being

$$w_{max} = U \max\left(\frac{x_p}{2\pi}, \frac{a}{2\pi}\right) \tag{13}$$

the maximum frequency of the integrand function.
An alternative expression for (11) can be:

$$\left\{\left[m_1, m_2\right], \left[m_2, m_3\right], \ldots, \left[m_{N_m - 1}, m_{N_m}\right]\right\} \tag{14}$$

S1.2.1 Adapted Gauss-Legendre quadrature (GLQ)

We want to restate Eq. (9) into an integral of the form:

$$\int_{-1}^{1} f(x)dx \simeq \sum_{i=1}^{n} w_i f(\chi_i)$$

where the points $\{\chi_i\}_{i=0}^{n}$ are the roots of the Legendre polynomial of degree n and $\{w_i\}_{i=0}^{n}$ are the associated weights (Hildebrand, 1956). We employ an adaptive algorithm to numerically solve Eq. (9). The support of the integral is partitioned into N_m (12) sub-intervals (14). The integral is then computed within each sub-interval setting $n = 3$. The values of the points and weights are (Hildebrand, 1956):

$$\begin{array}{lll} \chi_1 = -\sqrt{\frac{3}{5}} & \chi_2 = 0 & \chi_3 = \sqrt{\frac{3}{5}} \\ w_1 = \frac{5}{9} & w_2 = \frac{8}{9} & w_3 = \frac{5}{9} \end{array}$$

As the endpoints of the sub-intervals (Eq. 11) do not align with ± 1, a change of reference system is necessary, requiring a restatement of the integrand as follows:

$$f\left(m^{\frac{i}{2}} + m^{\frac{-i}{2}}\chi_j, U, a, x_p, H_0\right) = \frac{\cos\left(m^{\frac{i}{2}} + m^{\frac{-i}{2}}\chi_j U x_p\right)\sin\left(m^{\frac{i}{2}} + m^{\frac{-i}{2}}\chi_j U a\right)}{\left(m^{\frac{i}{2}} + m^{\frac{-i}{2}}\chi_j U\cosh\left(m^{\frac{i}{2}} + m^{\frac{-i}{2}}\chi_j U H_0\right)\right.} \tag{15}$$

having called:

$$m^{\frac{i}{2}} = \frac{m_i + m_{i+1}}{2} \tag{16}$$

$$m^{\frac{-i}{2}} = \frac{m_{i+1} - m_i}{2} \tag{17}$$

The free surface deformation will be approximated by:

$$\xi_0(x_p) \simeq U\frac{2B_0}{\pi}\left[\frac{a\epsilon}{U} + \sum_{i=1}^{N_m - 1} m^{\frac{-i}{2}} \sum_{j=1}^{3} w_j f\left(m^{\frac{i}{2}} + m^{\frac{-i}{2}}\chi_j, U, a, x_p, H_0\right)\right] \tag{18}$$

for all the points x_p in the LED (10).

S1.2.2 Adapted Filon quadrature (FQ)

Filon's quadrature is particularly advantageous for finding approximate solutions to highly oscillatory integrals of the form:

$$\int_0^\infty f(x)\cos(kx)dx, \quad \int_0^\infty f(x)\sin(kx)dx, \quad \int_0^\infty f(x)e^{i\omega x}dx$$

Here, f is a sufficiently smooth function that multiplies a sinusoid oscillating at high frequency $k \in \mathbf{R}$. The method involves replacing f with an interpolating polynomial, plus a remainder term, which allows for exact integration. Greater details can be found, for instance, in (Filon, 1930; Iserles, 2004). We would like to rewrite the integral in Eq. (1) as:

$$\int_\epsilon^U f(m)\sin(mx)dm \tag{19}$$

Reminding that:

$$\frac{1}{2}\Big[\sin(m(a+x)) - \sin(m(a-x))\Big] = \cos(ma)\sin(mx) \tag{20}$$

and scaling the support of the integral, Eq. (9) would be:

$$\xi_0(x_p) \simeq U\frac{B_0}{\pi}\int_{\frac{\epsilon}{U}}^{1}\frac{\sin(mU(a+x))}{mU\cosh(mUH)}dm - U\frac{B_0}{\pi}\int_{\frac{\epsilon}{U}}^{1}\frac{\sin(mU(a-x))}{mU\cosh(mUH)}$$

If we consider a discrete integral support as in Eq. (14), we restate the previous equation as:

$$\xi(x_p) \simeq U\frac{2B_0}{\pi}\left(\frac{a\epsilon}{U} + \frac{1}{2}\sum_{j=1}^{N_m-1}\frac{\sin(m_j(a+x_p))}{m_jU\cosh(m_jUH_0)} - \frac{1}{2}\sum_{j=1}^{N_m-1}\frac{\sin(m_jU(a-x_p))}{m_jU\cosh(m_jUH_0)}\right) \tag{21}$$

for all the points x_p in the LED (10). For the Filon quadrature, we used a subroutine available at the link https://people.sc.fsu.edu/~jburkardt/m_src/filon/filon.html.

S1.3 Comparison with Kajiura

We compare the sea surface deformations obtained by the application of a "Kajiura-type" filter with those given by a "Nosov-type" filter. The latter is evaluated through the Eq. (8), solved by the adapted Gauss-Legendre quadrature detailed in Section S1.2.1. The former is expressed as:

$$\xi_{kaj}(x) = \int_{-\infty}^{+\infty}\frac{\eta_0(x')}{\cosh(kH_0)}dx' \tag{22}$$

Equation (22) tells that the coseismic deformation η_0 is smoothed, at each point, by a factor $\frac{1}{\cosh(kH_0)}$, where k is the wavenumber and H_0 is the water depth, held constant along the segment or area where such deformation is evaluated.

S1.4 Superposition of unit contributions: validation of the linear assumption

Eq. (1), along with its equivalent scaled versions (9), are analytical solutions to the Laplace equation for the scalar potential of fluid velocity, assuming a flat bottom H_0. Under this hypothesis, the Laplace equation is linear and therefore the superposition principle holds. We show this through a systematic test, involving the extent of the coseismic deformations used in the main text (Section 3.1) ($a \simeq$ 11 km, 19 km, 26 km), each divided into unit cells of different lengths (15, 30, 60 arc-sec). The sea depth is assumed to be 1 km, 4 km, and 8 km. The sea surface maximum height resulting from different combinations of these parameters is compared against the reference solution, obtained by directly applying Eq. (9). The comparison reveal a very good agreement across all cases, with a minimum error of $\sim 10^{-4}$ m and a maximum error of $\sim 10^{-3}$ m, as depicted in Fig. S4.

S2 Laplacian Smoothing Tool - 1D case

The one dimensional Laplace Smoothing Tool (1D-LST hereafter) takes as input data the sea-bottom deformation and the sea-depth for a region of interest D. Both the inputs are expressed in geographic coordinates. We denote with λ the latitude and with ϕ the longitude. The coseismic deformation and the water depth are functions $z(\phi, \lambda)$ of the geographic points in the grid. The 1D-LST can be summarized in the following two steps.

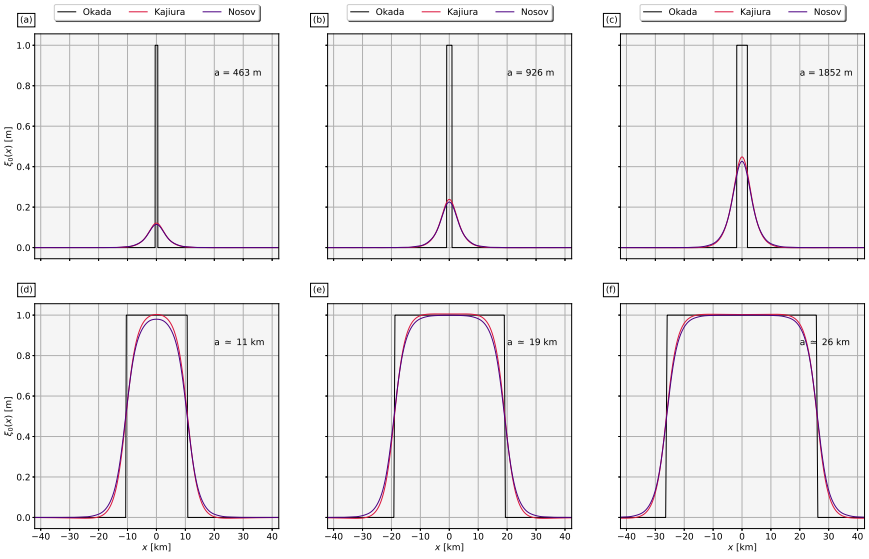

Figure S2. The free surface perturbations obtained by applying the standard procedure (which consists in copying the coseismic deformation at the sea surface), the Kajiura-type filter and the Nosov-type filter are compared, assuming a constant water depth and varying the extent of the seafloor deformation.

Step 1

Given a starting point (λ_0, ϕ_0) and end ending point (λ_1, ϕ_1) in the grid, a 1D transect is extracted for both the sea-depth and the coseismic deformation. In cartesian coordinates, the initial and ending points of the transect will be given by (x_0, y_0) and (x_1, y_1). Both the sea depth and the seafloor deformation along the transect are discretized into a finite number N_c of cells, according to the desired resolution. Once the cell length a is fixed, each cell is resampled into a certain number of points N_x. Equation (9) is evaluated at each point x_p in the cell. The resampled grid step is given by:

$$dx = \frac{2a}{N_x} \tag{23}$$

The 1D sea depth and seafloor deformation profiles are interpolated in the new domain:

$$\widetilde{D} = 0, dx, 2dx, \ldots, \sqrt{(x_1 - x_0)^2 + (y_1 - y_0)^2} \tag{24}$$

which consists of a number N_c of cells given by:

$$N_c = \frac{\sqrt{(x_1 - x_0)^2 + (y_1 - y_0)^2}}{2a} \tag{25}$$

Practically, N_c is rounded to an integer. Since both the coseismic deformation and the sea-depth are assumed to be constant within each cell c_i, an average value is taken among the N_x interpolated values, resulting in the two sets $\left\{B_0^i\right\}_{i=1}^{N_c}$ and $\left\{H_0^i\right\}_{i=1}^{N_c}$.

Step 2

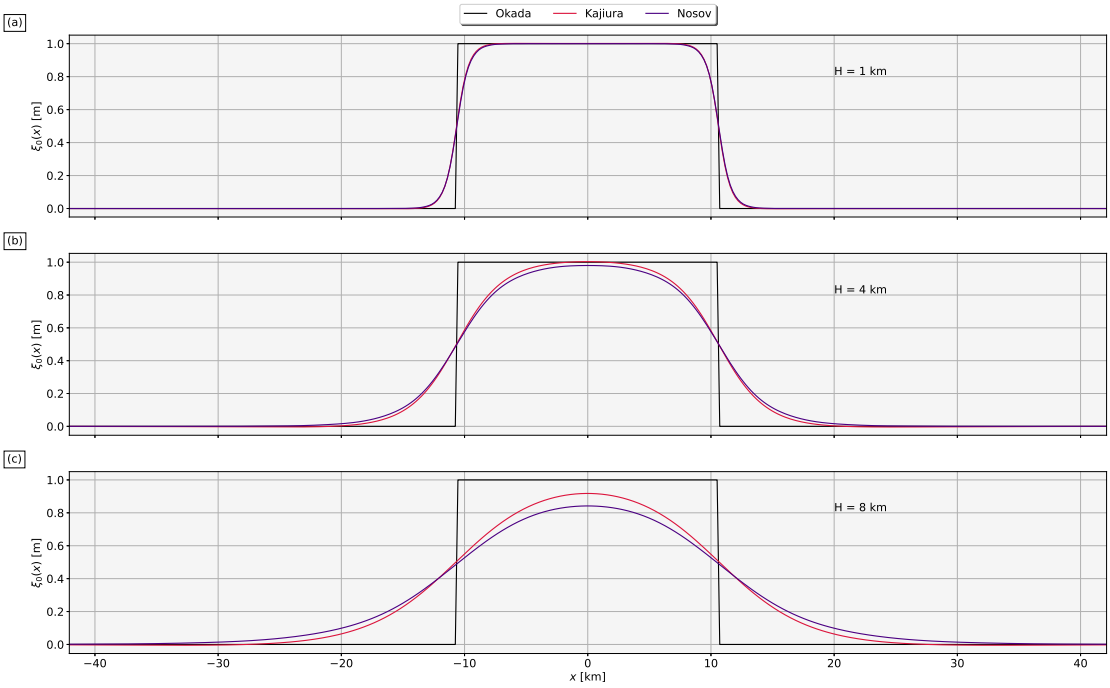

Figure S3. The same of Fig S2, but helding constant the extent of the coseismic deformation and varying the water depth.

For each cell c_i, Eq. (9) is solved in the associated LED (10) through an adapted Gauss-Legendre formula (18), as detailed previously in Section S1.2.1. Since the LED is centered in zero, the within-cell sea surface deformation ξ_0^i is shifted and interpolated to match the nodes in $\widetilde{D}$. The final free surface perturbation ξ_0 is given by summing, at each iteration, the within-cell sea surface deformation ξ_0^i. A pseudo-code for the 1D-LST is provided in the following section.

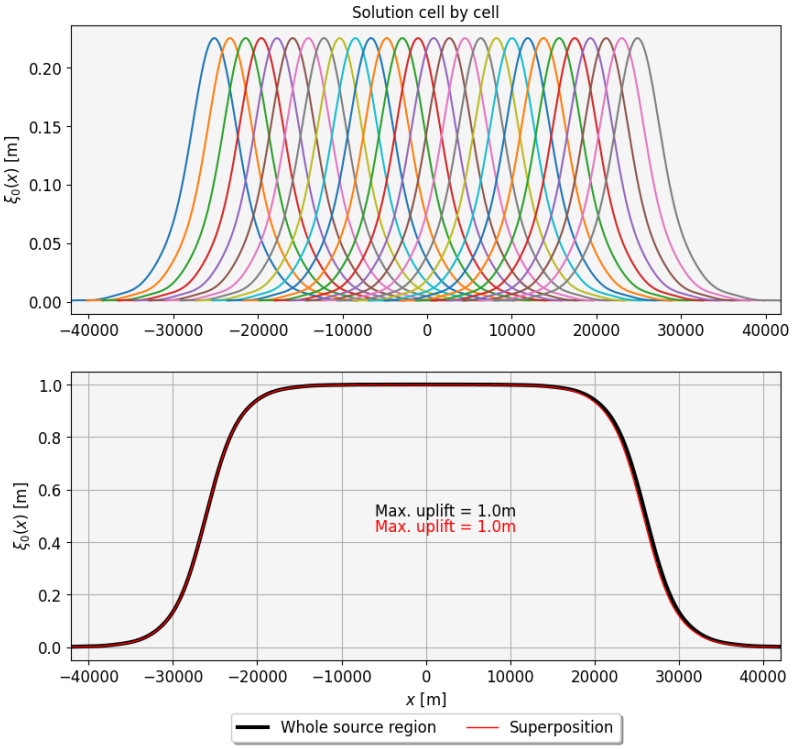

Figure S4. The LED (10) associated to a coseismic deformation of about 26 km is partitioned into cells of equal size a ∼920 m (∼30 arc-sec). Sea-bottom deformation and water depth are fixed at $B_0 = 1$ m and H_0 =4 km, respectively. The upper panel displays the water height within each cell, while the lower panel illustrates the comparison between the superposition of unit cells (depicted in red) and the resulting free-surface perturbation, obtained by directly solving the Eq. (9) across the entire source.

S2.0.1 Pseudo code

Algorithm 1 1D-LST

Input: Sea-depth within the domain and amplitude of the coseismic deformation, both provided as a ".xyz" files having as entries (LON, LAT, ELEVATION)

Output: 1D Filtered free surface deformation in cartesian coordinates

$\phi, \lambda, H \leftarrow$ Longitude, Latitude, Sea-depth

$\phi, \lambda, B_0 \leftarrow$ Longitude, Latitude, Amplitude of the seafloor deformation

Ensure: H is positive downward

Get a transect of H and B_0 starting from a point (ϕ_0, λ_0) and an ending at (ϕ_1, λ_1) and convert it to Cartesian coordinates, such that the first point is (x_0, y_0) and the last one is (x_1, y_1)

Set a value for a, depending on the resolution required

$N_x \leftarrow 5$

$dx \leftarrow \frac{2a}{N_x}$

$\widetilde{D} \leftarrow 0, dx, 2dx, \ldots, \sqrt{(x_1 - x_0)^2 + (y_1 - y_0)^2}$

Inizialize an array for the final filtered free surface ξ_0, obtained by linearly combine unit contributions, having the same dimension of $\widetilde{D}$

$N_c \leftarrow round(\frac{\max(D_x) - \min(D_x)}{2a})$

Interpolate both B_0 and H in $\widetilde{D}$

for each cell i **do**

  if $H[i] > 0$: **then**

    Define the LED l_e^i as in Eq. 10

    Solve the elementary contribution ξ_0^i in l_e^i through the Adapted Gauss-Legendre (18)

    $x_{\text{shift}} \leftarrow \widetilde{D}[N_x * i]$

    $l^i_{e,\text{shifted}} \leftarrow l_e^i + x_{\text{shift}}$ to shift the LED, such that its center is not zero

    $i_{new} \leftarrow N_x * i - \text{round}(\frac{4H_0^{ij}}{2dx})$

    $i_D \leftarrow D_x[i_{new} : i_{new} + \text{round}(\frac{8H_0^{ij} + 2*\max(a,b)}{dx})]$ to find the correct position of the unit contribution in the domain

    $\xi^i_{interp} \leftarrow$ interpolate each unit solution ξ_0^j in the real nodes of the grid i_D

    $iX_{min} \leftarrow i_{new}$

    $iX_{max} \leftarrow i_{new} + \text{round}(\frac{8H_0^{ij} + 2\max(a,b)}{dx})$

    $\xi_0[iX_{min} : iX_{max}] \pm B_0^i \times \xi^i_{interp}$

  end if

end for

Down-sample ξ_0 to have the same length of the original transect, by taking the average value over windows of N_x points

S3 The 2D case

S3.1 Adapted Gauss-Legendre quadrature

In two dimensions, the free surface elevation is given by (Nosov and Kolesov, 2011):

$$\xi(x,y) = \frac{4B_0}{\pi^2} \int_0^\infty dm \int_0^\infty dn \frac{\cos(mx)\sin(ma)\cos(ny)\sin(nb)}{mn\cosh(kH_0)} \tag{26}$$

where a is the extension of the coseismic deformation along $\hat{x}$, b is the width of the coseismic deformation along $\hat{y}$, (x, y) is a point in the domain and $k = \sqrt{m^2 + n^2}$. B_0 is the amplitude of the residual bottom deformation and H_0 is the water depth, taken as positive downward, both assumed to be constant inside the rectangle with borders a and b.

The methodology adopted is a natural extension of the 1D case proposed in Section 2.1 and consists of an adaptive Gauss-Legendre quadrature evaluated at four points, considered to be enough for this application.

The equivalent scaled version of Eq. (26) is:

$$\xi_0(x,y) \simeq U^2 \frac{4B_0}{\pi^2} \left(\frac{ab\epsilon}{U^2} + O(\epsilon^4) + \int_{\frac{\epsilon}{U}}^{1} \int_{\frac{\epsilon}{U}}^{1} \frac{\cos(Umx)\sin(Uma)\cos(Uny)\sin(Unb)}{mnU^2\cosh(kUH)} dmdn \right) \tag{27}$$

Given D an ocean basin, we discretize it into a finite number N_c^x x N_c^y of cells $\{c_{ij}\}$, with constant length $2a$ along $\hat{x}$ and constant width $2b$ along $\hat{y}$. In each cell c_{ij} the sea-floor deformation B_0^{ij} and water depth H_0^{ij} are assumed to be constant. In two dimensions, the LED is defined by a rectangular area surrounding the cell in the Cartesian plane:

$$p_{min} = -4H_0^{ij} - \max(\frac{a}{2}, \frac{b}{2}) \tag{28}$$

$$p_{max} = 4H_0^{ij} + \max(\frac{a}{2}, \frac{b}{2}) \tag{29}$$

$$l_e^x = p_{min},\ p_{min} + \Delta x,\ p_{min} + 2\Delta x, \ldots,\ p_{max} - \Delta x,\ p_{max} \tag{30}$$

$$l_e^y = p_{min},\ p_{min} + \Delta y,\ p_{min} + 2\Delta y, \ldots,\ p_{max} - \Delta y,\ p_{max} \tag{31}$$

where Δx and Δy are the spacing between the points along the $\hat{x}$ and $\hat{y}$ directions respectively. The number of points in (28) is:

$$N_x = \frac{2a}{\Delta x}$$
$$N_y = \frac{2b}{\Delta y}$$

The number of cells along the two directions is:

$$N_c^x = \frac{p_{max} - p_{min}}{2a} \tag{32}$$

$$N_c^y = \frac{p_{max} - p_{min}}{2b} \tag{33}$$

Practically, both N_c^x and N_c^y are rounded to integers.

The initial condition given by Eq. (27) is solved numerically at every point (x_e, y_e) of the LEDs (28) associated to the respective cell c_{ij}.

As done in Section S1.2, the partition of the integral support $\left[\frac{\epsilon}{U}, 1\right] \times \left[\frac{\epsilon}{U}, 1\right]$ should be chosen according to the numerator $g(mU, x, a)h(nU, y, b)$ of the integrand function, with $g(mU, x, a) = \cos(mUx)\sin(mUa)$ and $h(nU, y, b) = \cos(nUy)\sin(nUb)$. In two dimension, this can be achieved by independently dividing each of the two supports into a number of points controlled by the maximum oscillation frequencies w_{max}^g of g and w_{max}^h of h, respectively.

The maximum frequencies are defined as:

$$w_{max}^g = U \max\left(\frac{x_e^{p_x}}{2\pi}, \frac{a}{2\pi}\right) \quad \forall p_x = 1, \dots, N_x \tag{34}$$

$$w_{max}^h = U \max\left(\frac{y_e^{p_y}}{2\pi}, \frac{b}{2\pi}\right) \quad \forall p_y = 1, \dots, N_y \tag{35}$$

and the number of sub-intervals for the support $\left[\frac{\epsilon}{U}, 1\right] \times \left[\frac{\epsilon}{U}, 1\right]$, according to the maximum frequencies, are given by:

$$N_m = \max\left[2w_{max}^g, N_s\right] \tag{36}$$

$$N_n = \max\left[2w_{max}^h, N_s\right] \tag{37}$$

for the integration with respect to m, along $\hat{x}$ and with respect n, along $\hat{y}$ respectively, for each point $(x_e^{p_x}, y_e^{p_y})$ in the LED 28. In Eq. (36) $N_s = 10$ to properly capture the sinusoidal cycles.

The free surface deformation is numerically approximated by:

$$\xi_0(x_p, y_p) \simeq U \frac{4B_0}{\pi^2}\left[\frac{ab\epsilon^2}{U^2} + \sum_{j=1}^{N_n-1}\sum_{i=1}^{N_m-1} n_j^{-\frac{1}{2}} m_i^{-\frac{1}{2}} \sum_{k=1}^{4} w_k f\left(n_j^{\frac{1}{2}} + n_j^{-\frac{1}{2}}\chi_k^x, m_i^{\frac{1}{2}} + m_i^{-\frac{1}{2}}\chi_k^y, U, a, b, x_p, y_p, H_0\right)\right] \tag{38}$$

for all $x_p \in l_e^{\hat{x}}$ and $y_p \in l_e^{\hat{y}}$, having called:

$$f(n, m, U, a, b, x_p, y_p, H_0) = \frac{\cos(mUx_p)\sin(mUa)\cos(nUy_p)\sin(nUb)}{mnU^2\cosh(kUH_0)}$$

$$n_j^{\frac{1}{2}} = \frac{n_j + n_{j+1}}{2} \quad j = 1, \dots, N_n - 1$$

$$n_j^{-\frac{1}{2}} = \frac{n_{j+1} - n_j}{2} \quad j = 1, \dots, N_n - 1$$

$$m_i^{\frac{1}{2}} = \frac{m_i + m_{i+1}}{2} \quad i = 1, \dots, N_m - 1$$

$$m_i^{-\frac{1}{2}} = \frac{m_{i+1} - m_i}{2} \quad i = 1, \dots, N_m - 1$$

The points χ_k and weights w_k for the quadrature rule are given by:

$$\chi_k^x = \left[\frac{-1}{\sqrt{3}}, \frac{-1}{\sqrt{3}}, \frac{1}{\sqrt{3}}, \frac{1}{\sqrt{3}}\right]$$
$$\chi_k^y = \left[\frac{-1}{\sqrt{3}}, \frac{1}{\sqrt{3}}, \frac{-1}{\sqrt{3}}, \frac{1}{\sqrt{3}}\right]$$
$$w_k = [1, 1, 1, 1]$$

S3.2 Physical Interpretation: 2D unit sources with varying parameters

In Fig. S5, we present the 2D unit sea surface height described in the main text (Section 3.1). We first held constant the water depth at 4 km and let the cell size vary. Specifically, the length of the cell a is assumed 15 arc-sec, 30 arc-sec, 60 arc-sec, 11 km, 19 km, and 26 km, and the width $b = \frac{a}{2}$. Finally, we consider a fixed cell size of $a \simeq 11$ km and a varying depth of 1 km, 4 km, and 8 km.

S3.3 Laplacian Smoothing Tool - 2D case

The LST (Laplacian Smoothing Tool) in two dimensions (hereafter denoted as 2D-LST) consists of three steps, each of them discussed in the following.

Step 1

The input data consists of the sea-depth, provided in geographic coordinates at a certain resolution. A change of reference system is executed, transitioning from geographic to UTM. The sea-depth is discretized into a finite number of cells $N_c^x \times N_c^y$. To keep unchanged the resolution at which the sea-depth is originally given, we set as $\frac{a}{2}$, the size of the cell along $\hat{x}$, and $\frac{b}{2}$, the size of the cell along $\hat{y}$, equal to the mean differences between the nodes of the grid in the two respective directions. Each cell is resampled into a certain number of points $N_x \times N_y$. The resampled grid step is given along the two directions of the cartesian plane by:

$$dx = \frac{2a}{N_x} \tag{39}$$
$$dy = \frac{2b}{N_x} \tag{40}$$

The domain D where the sea surface perturbation is evaluated has components:

$$D_x = x_0, dx, 2dx, \ldots, x_N \tag{41}$$
$$D_y = y_0, dy, 2dy, \ldots, y_M \tag{42}$$

where N_c^x and N_c^y are the number of cells in the two directions, given by:

$$N_c^x = \frac{x_N - x_0}{2a} \tag{43}$$
$$N_c^y = \frac{y_M - x_0}{2b} \tag{44}$$

Practically, both N_c^x and N_c^y are rounded to integer numbers.

Step 2

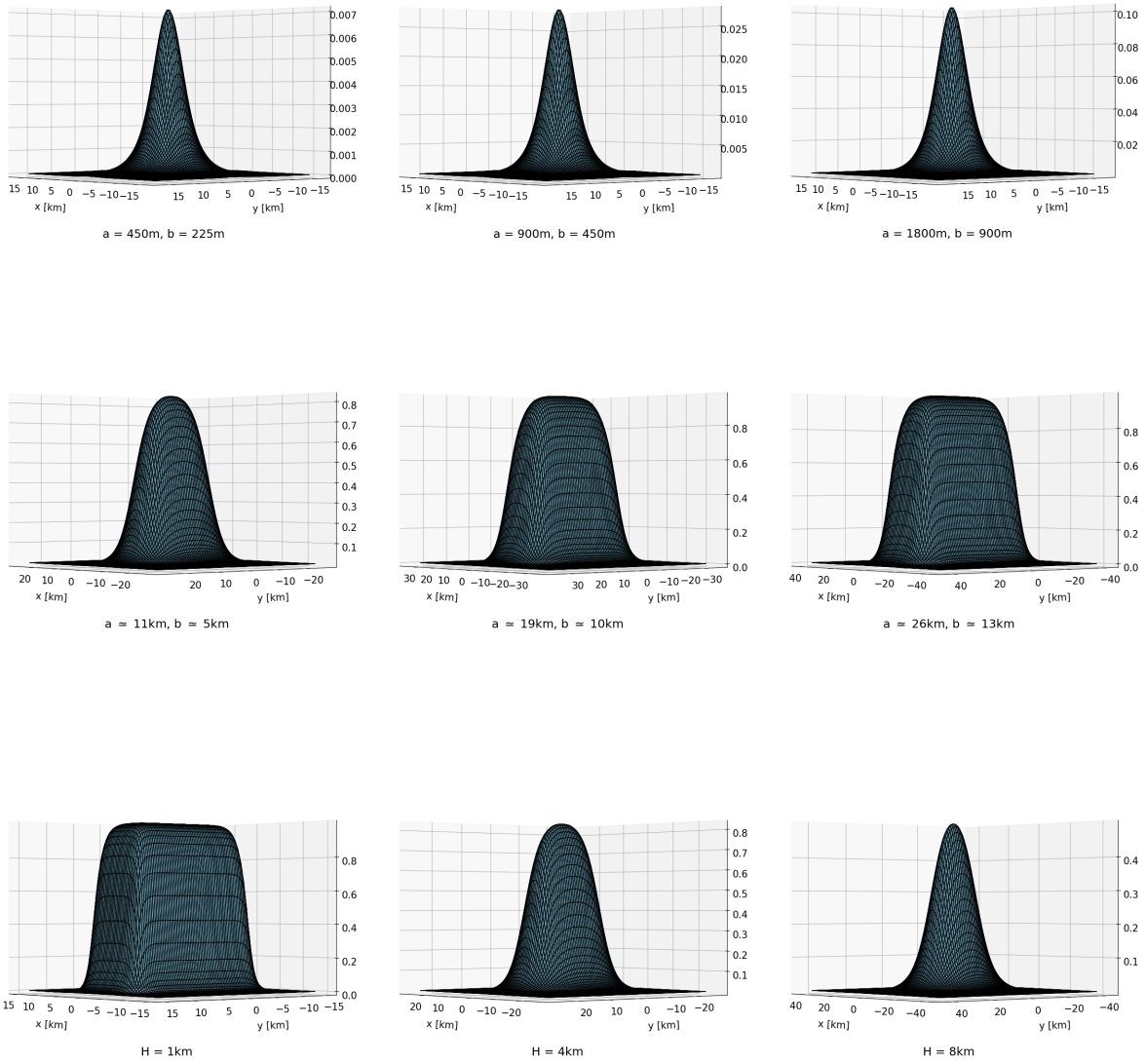

Figure S5. 2D shapes as model parameters change. The first six graphs, in which only the cell dimensions are shown in each title, are obtained by keeping the water depth constant. The last three graphs share the same cell dimensions and consider a varying water depth

Equation (27) is solved within the LED associated to each cell, scaled by the respective sea-floor deformation. The integration is performed according to the adapted Gauss-Legendre quadrature detailed in Section (S3.1). This approach enables the creation of a database for the region of interest at a specific resolution, facilitating reuse across various applications. Although the proposed numerical scheme for integral solving is highly efficient, addressing high resolutions and extensive domains can lead to time-consuming operations when solving the integral within each cell. To enhance computational speed, each cell can be independently solved by exploiting the High-Performance Computing (HPC) resources.

Step 3

Final results can be merged and combined to obtain the final filtered free-surface deformation. For each cell, we retrieve the result obtained from integration in its LED and re-scale it according to the value of the residual seafloor deformation. Similarly to the 1D case (see Section 3), since the LEDs are centered in zero, the within-cell sea surface deformation ξ_0^{ij} associated to each cell c_{ij} is shifted and interpolated to match the nodes in D_x and D_y. The final free surface perturbation ξ_0 is given by summing, at each iteration, the within-cell sea surface deformation ξ_0^{ij}. A pseudo-code for the 2D-LST is provided in the following section.

S3.3.1 Pseudo code

Algorithm 2 Step 1
Input: Sea depth within the domain, provided as a ".xyz" file having as entries (LON, LAT, ELEVATION)
Output: Cartesian Coordinates, grid for the filtered free-surface deformation and number of cells

$\phi, \lambda, H \leftarrow$ Longitude, Latitude, Sea-depth
Ensure: H is positive downward
$x, y \leftarrow$ convertToUTM(λ, ϕ)
a is set as half the average spacing between values in x
b is set as half the average spacing between values in y
The number of points to resample each cell is $N = 5$
$dx \leftarrow \frac{2a}{N}$
$dy \leftarrow \frac{2b}{N}$
$D_x \leftarrow \min(x), \min(x) + dx, \min(x) + 2dx, \ldots, \max(x)$
$D_y \leftarrow \min(y), \min(y) + dy, \min(y) + 2dy, \ldots, \max(y)$
$N_c^x \leftarrow round(\frac{\max(D_x) - \min(D_x)}{2a})$
$N_c^y \leftarrow round(\frac{\max(D_y) - \min(D_y)}{2b})$

Algorithm 3 Step 2
Input: Sea depth within the domain, outputs from Step 1, indices i, j denoting which cell we are referring to
Output: Local database of unit sources in Cartesian Coordinates, constructed through a job-array in a cluster

$B_0 \leftarrow 1$
if $H[i, j] > 0$: **then**
    Define the LED l_e^x along $\hat{x}$
    Define the LED l_e^y along $\hat{y}$
    Evaluate the elementary contribution for the ξ_0^{ij} using the GLQ (adapted Gauss-Legendre Quadrature) scheme
    Save l_e^x, l_e^y, ξ_0^{ij} in a netCDF file "cell_i_j.nc"
end if

Algorithm 4 Step 3

Input: Amplitude of the coseismic deformation B_0, Sea-depth within the domain, outputs from Step 1, path to the local database (*pathToDir*)

Output: Filtered free surface ξ_0 in the original Geographic coordinates

Upload $B_0, D_x, D_y, a, b, dx, dy, N_c^x, N_c^y, N$

Inizialize an array ξ_0 having dimensions $(len(D_x), len(D_y))$, which represents the final free-surface

for all the files "cell_i_j.nc" in pathToDir **do**

Retrieve l_e^x, l_e^y, ξ_0^{ij}

$x_{shift}, y_{shift} \leftarrow D_x[N*i], D_y[N*j]$

$l^x_{e,shifted} \leftarrow l_e^x + x_{shift}$

$l^y_{e,shifted} \leftarrow l_e^y + y_{shift}$

$i_{new} \leftarrow N*i - \text{round}(\frac{4H_0^{ij}}{2dx})$

$j_{new} \leftarrow N*j - \text{round}(\frac{4H_0^{ij}}{2dy})$

$i_D \leftarrow D_x[i_{new} : i_{new} + \text{round}(\frac{8H_0^{ij}+2*\max(a,b)}{dx})]$

$j_D \leftarrow D_y[j_{new} : j_{new} + \text{round}(\frac{8H_0^{ij}+2*\max(a,b)}{dy})]$

$\xi^{ij}_{interp} \leftarrow$ interpolate each unit solution ξ_0^{ij} in the real nodes of the grid i_D, j_D

$iX_{min} \leftarrow i_{new}$

$iX_{max} \leftarrow i_{new} + \text{round}(\frac{8H_0^{ij}+2\max(a,b)}{dx}) + N_x$

$iX_{max} \leftarrow i_{new} + \text{round}(\frac{8H_0^{ij}+2\max(a,b)}{dx}) + N_x$

$iY_{max} \leftarrow j_{new} + \text{round}(\frac{8H_0^{ij}+2\max(a,b)}{dx}) + N_y$

$\xi_0[iX_{min} : iX_{max}, iY_{min} : iY_{max}] \pm B_0^{ij} * \xi^{ij}_{interp}$

end for

Down-sample ξ_0 to match the dimensions of the original domain D, by taking the average value over blocks of (N, N) points

S3.4 Test on real cases

S3.5 Relative percentage differences

We show the spatial distribution of Relative Percentage Differences (RPD) between the unfiltered and filtered initial conditions for all models described in the main text (Section 4.1). The RPD is defined by:

$$RPD = 100 \times \left| \frac{\xi_0^{LST} - \xi_0^{unf}}{\xi_0^{unf}} \right| \tag{45}$$

where ξ_0^{LST} is the initial free surface obtained through LST and ξ_0^{unf} is the unfiltered free surface deformation, obtained by copying the coseismic deformation at the free surface. Figure S6 depicts the results for the megathrust event occurred in late 2006. Figures S7 and S8 show the case of the 2007 outer-rise, considering the northwest-dipping and the southeast-dipping source models, respectively.

S3.6 Comparison between 2D-LST and Kajiura-type filter

As a term of comparison with the algorithm presented in this study, a Kajiura-type filter is applied to the resulting deformations, assuming a constant basin sea-depth of 2.5 km for the 2006 megathrust and of 7 km for the outer-rise, respectively. These values are approximately the averaged sea-depths along the area deformed by the shocks. The results for the 2006 event are illustrated in Fig. S9. Figure S10 shows the 1D profiles along the transect AB depicted Fig. S9a for all the nine models. For the 2007

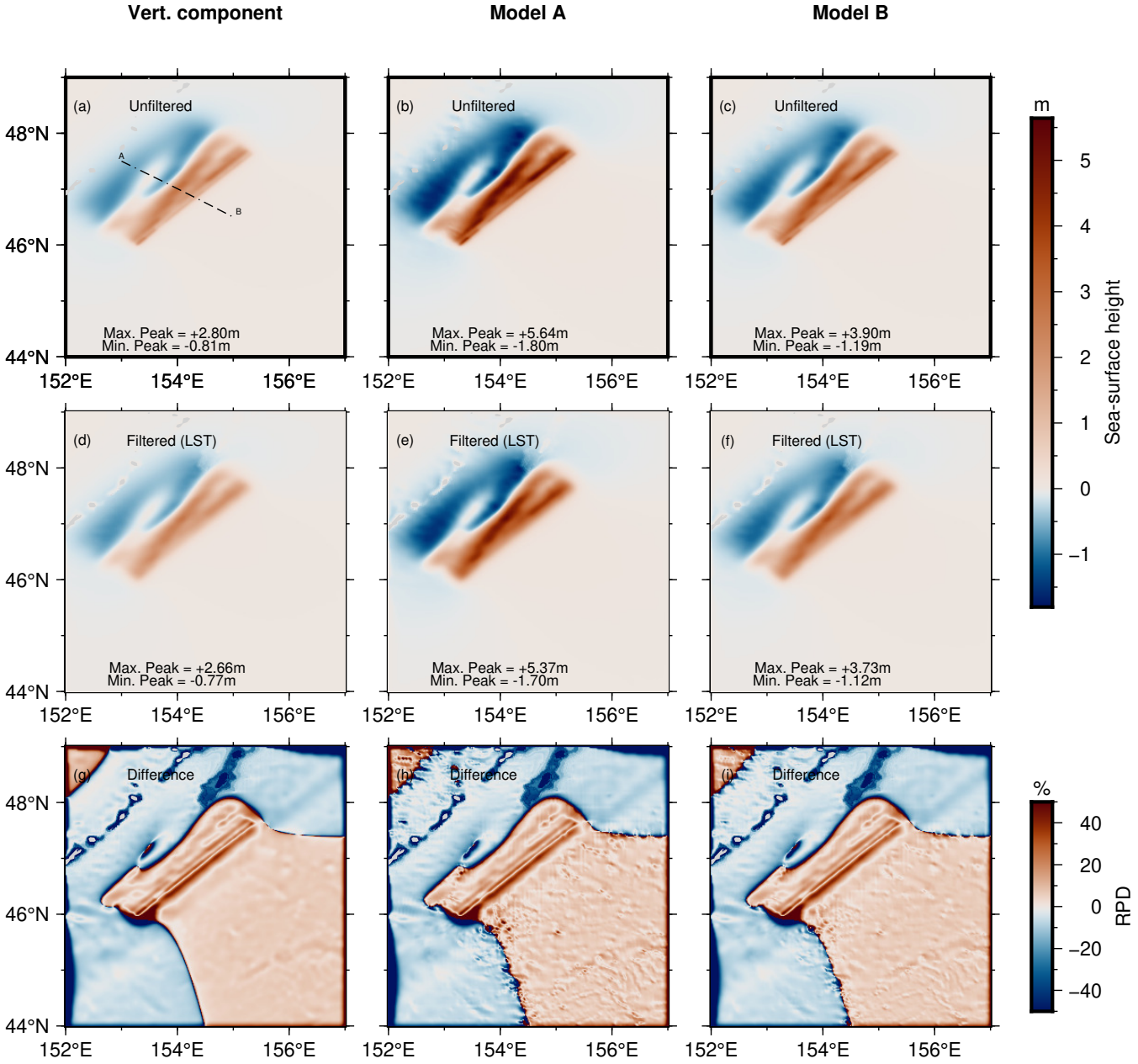

Figure S6. Results for the tsunamigenic earthquake occurred on November 15, 2006. The first column depicts the sea-surface distribution arising from a vertical bottom movement. The last two columns present the results obtained with the contribution of the horizontal bottom displacement according to Model A and Model B in Tanioka and Seno (2001). Panel (a) depicts the transect AB where 1D profiles for all the six models have been considered. Panels (g), (h) and (i) show how the RPD defined in Eq. (45) between the unfiltered and the filtered (LST) initial conditions are spatially distributed.

event, the outcomes for the northwest dipping fault plane are depicted in Fig. S11 and in Fig. S12. Findings for the southeast dipping fault plane are presented in Fig. S13 and in Fig. S14.

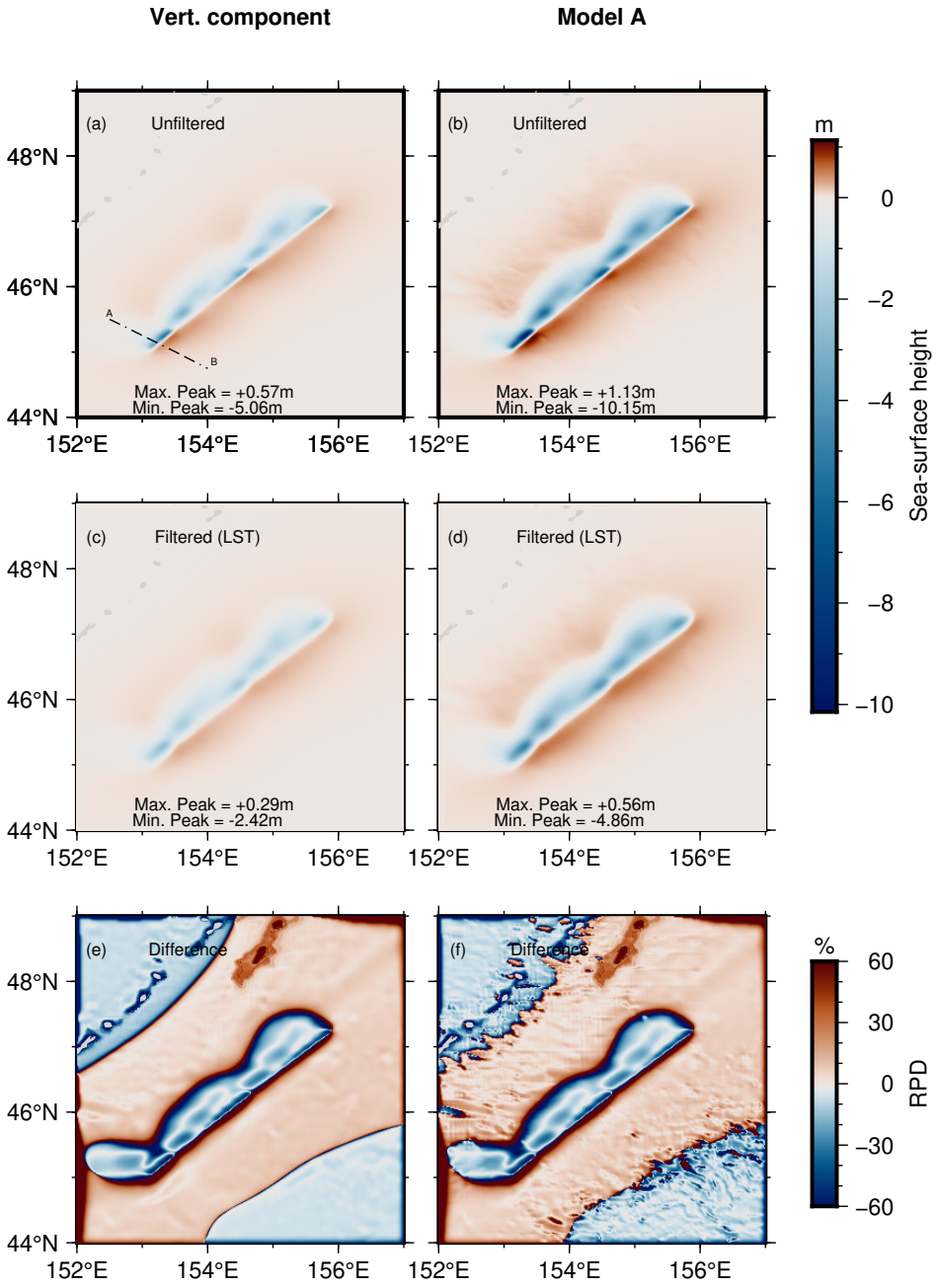

Figure S7. Results for the tsunamigenic earthquake occurred on January 13, 2007. The fault plane is northwest dipping. Panel (a) depicts the transect AB where 1D profiles for all models have been considered. Panels (e) and (f) show how the RPD defined in Eq. (45) between the unfiltered and the filtered (LST) initial conditions are spatially distributed.

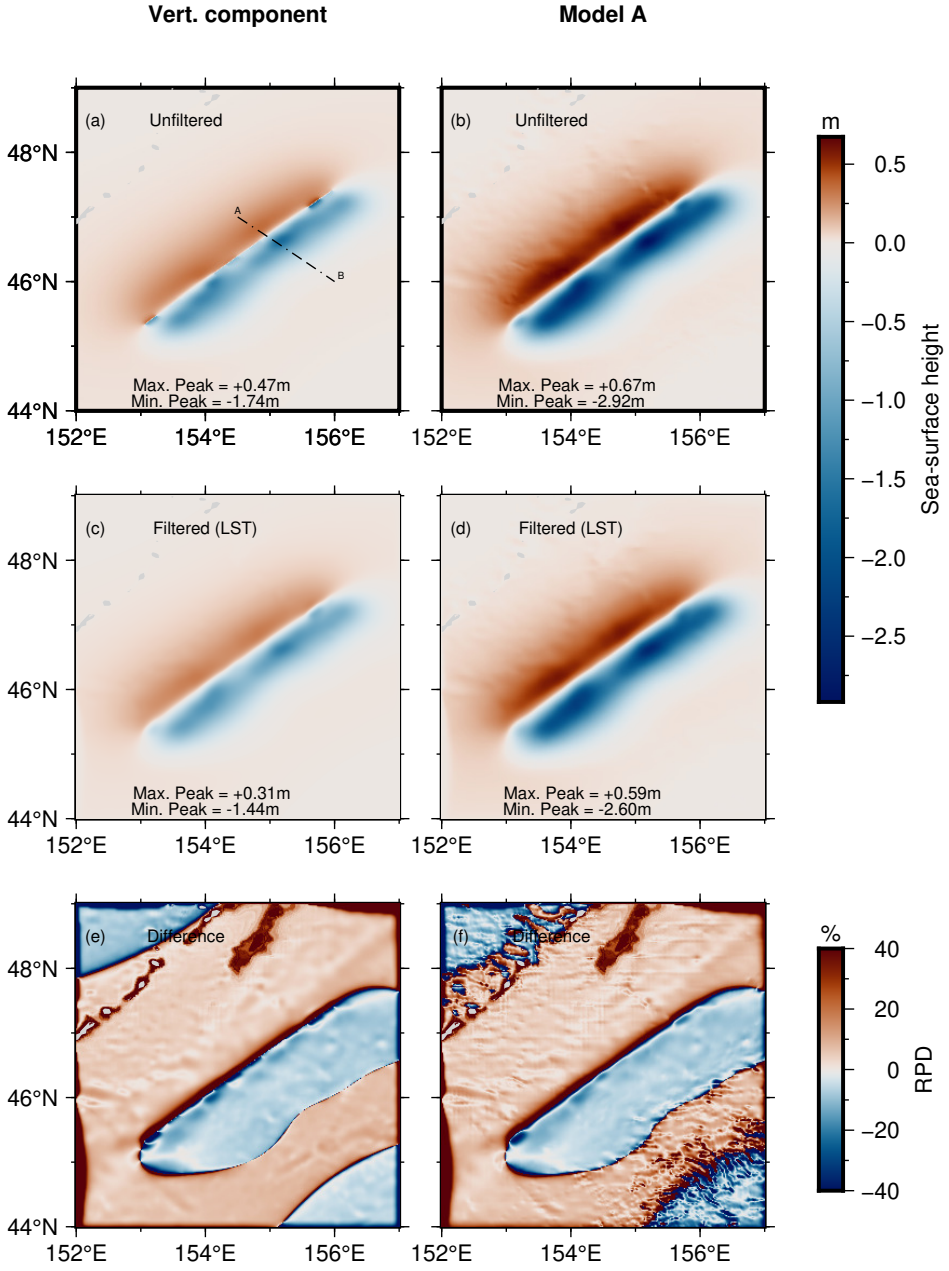

Figure S8. Results for the tsunamigenic earthquake occurred on January 13, 2007. The fault plane is southeast dipping. Panel (a) depicts the transect AB where 1D profiles for all models have been considered. Panels (e) and (f) show how the RPD defined in Eq. (45) between the unfiltered and the filtered (LST) initial conditions are spatially distributed.

S3.6.1 Comparison between 1D-LST and 2D-LST

We apply both the 1D-LST (Section S2) and 2D-LST (Section S3.3) to each of the models detailed in the Main Text (Section 4) and compare the results along three transects. Figures S15, S16 and S17 showcase the results for the 2006 megathrust event.

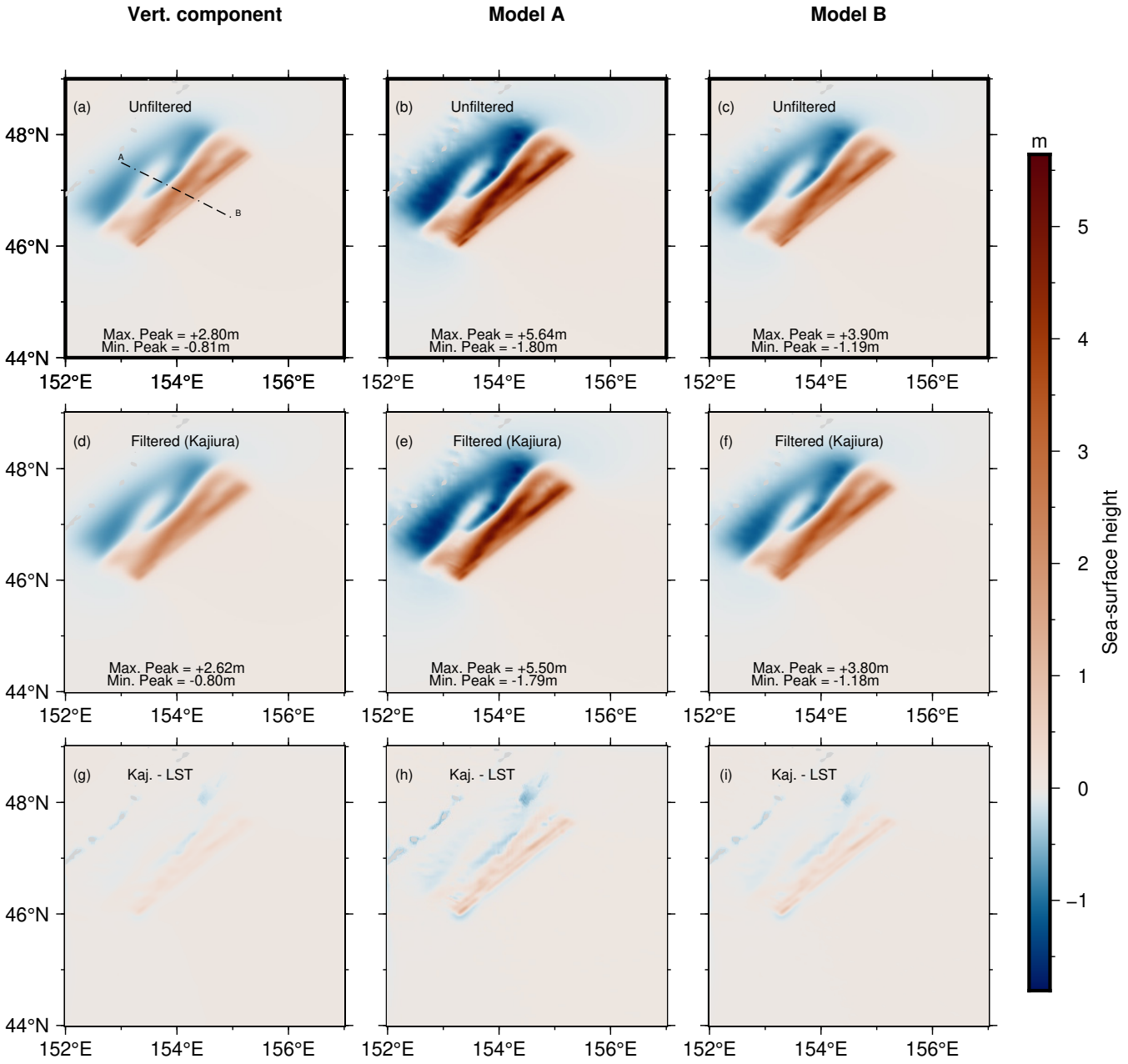

Figure S9. Results for the tsunamigenic earthquake occurred on November 15, 2006. The first column depicts the sea-surface distribution arising from a vertical bottom movement. The last two columns present the results obtained with the contribution of the horizontal bottom displacement according to Model A and Model B in Tanioka and Seno (2001). Panel (a) depicts the transect AB where 1D profiles for all the six models have been considered. Panels (g), (h) and (i) show how the simple differences between the initial conditions filtered with Kajiura and LST are spatially distributed.

Figures S18 and S19 depict the case of the 2007 outer-rise, considering a northwest oriented source. Figures S20 and S21 refer to the southeast-dipping model for the same event. In all the figures the unfiltered free-surface deformation is also plotted.

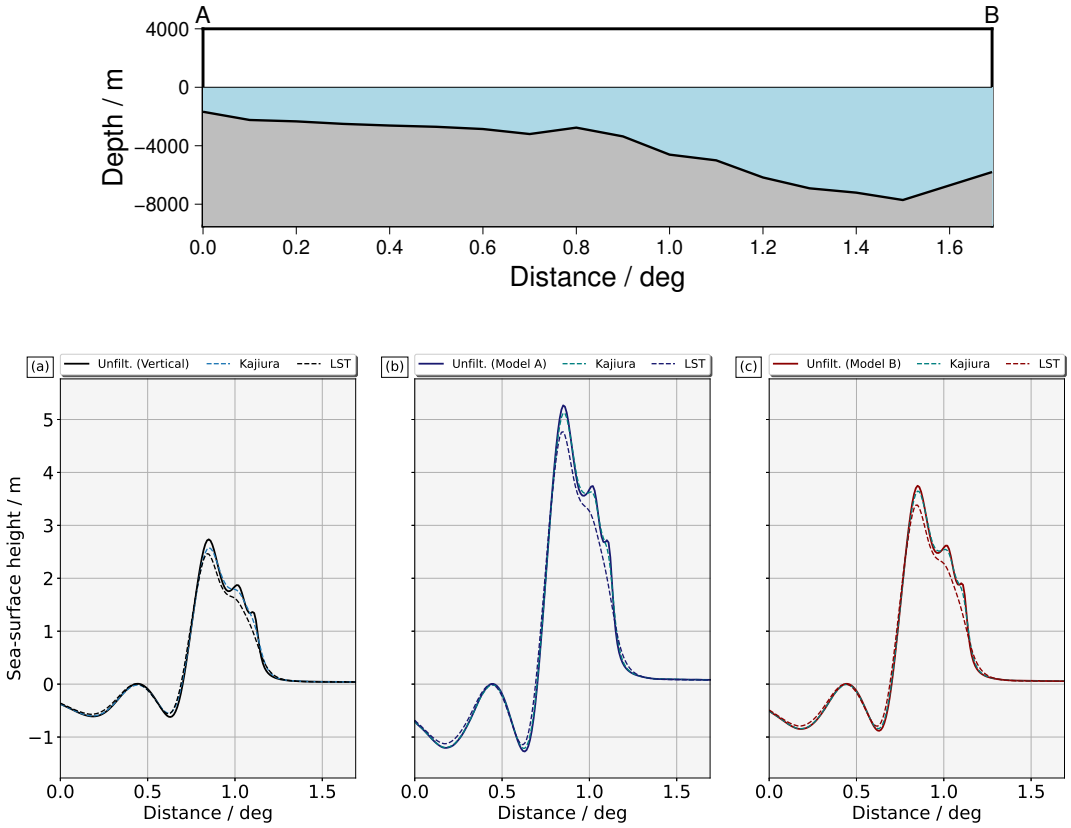

Figure S10. The transect AB under consideration is depicted in Fig. S9a. The upper panel illustrates the bathymetric profile. In (a), the profiles are derived from the initial conditions shown in Fig. S9 (a, d, g), taking into account only the vertical component. In (b), the profiles are obtained from the initial conditions in Fig. S9 (d, e, h), incorporating the influence of the horizontal component through Model A. Lastly, in (c), the profiles are extracted from the initial conditions in Fig. S9 (c, f, i), considering the effect of the horizontal component through Model B.

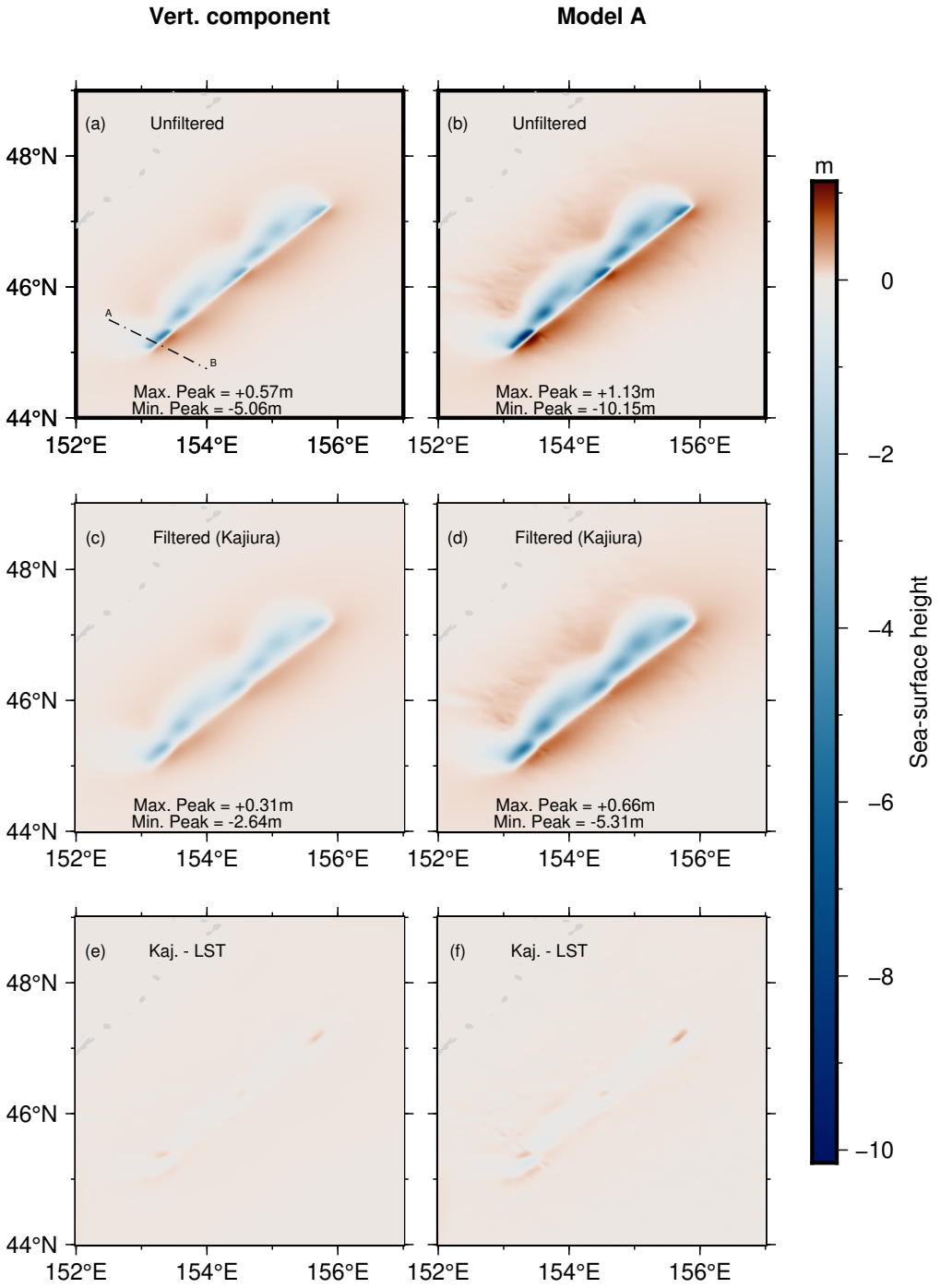

Figure S11. Results for the tsunamigenic earthquake occurred on January 13, 2007. The fault plane is northwest dipping. Panel (a) depicts the transect AB where 1D profiles for all models have been considered. Panels (e) and (f) show the spatial distributions of the simple differences between the initial conditions obtained by the application of the Kajiura-type filter and LST.

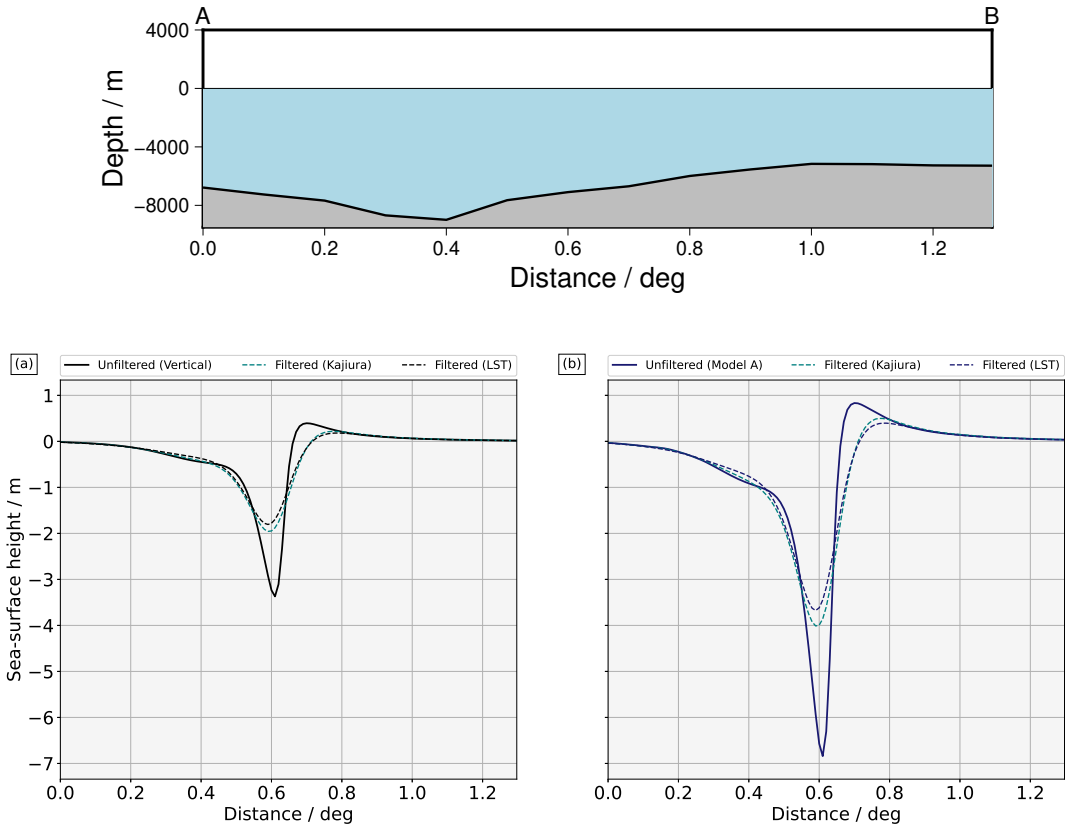

Figure S12. The picture refers to the 2007 event in case of a source oriented to the northwest. The transect AB considered is the one depicted in Fig. S11a. The upper panel illustrates the bathymetric profile along it. (a) The profiles are taken from the initial conditions in Figure S11 (a, c, e), considering only the vertical component. (b) The profiles are taken from the initial conditions in Figure S11 (b, d, f), considering the effect of the horizontal component through Model A.

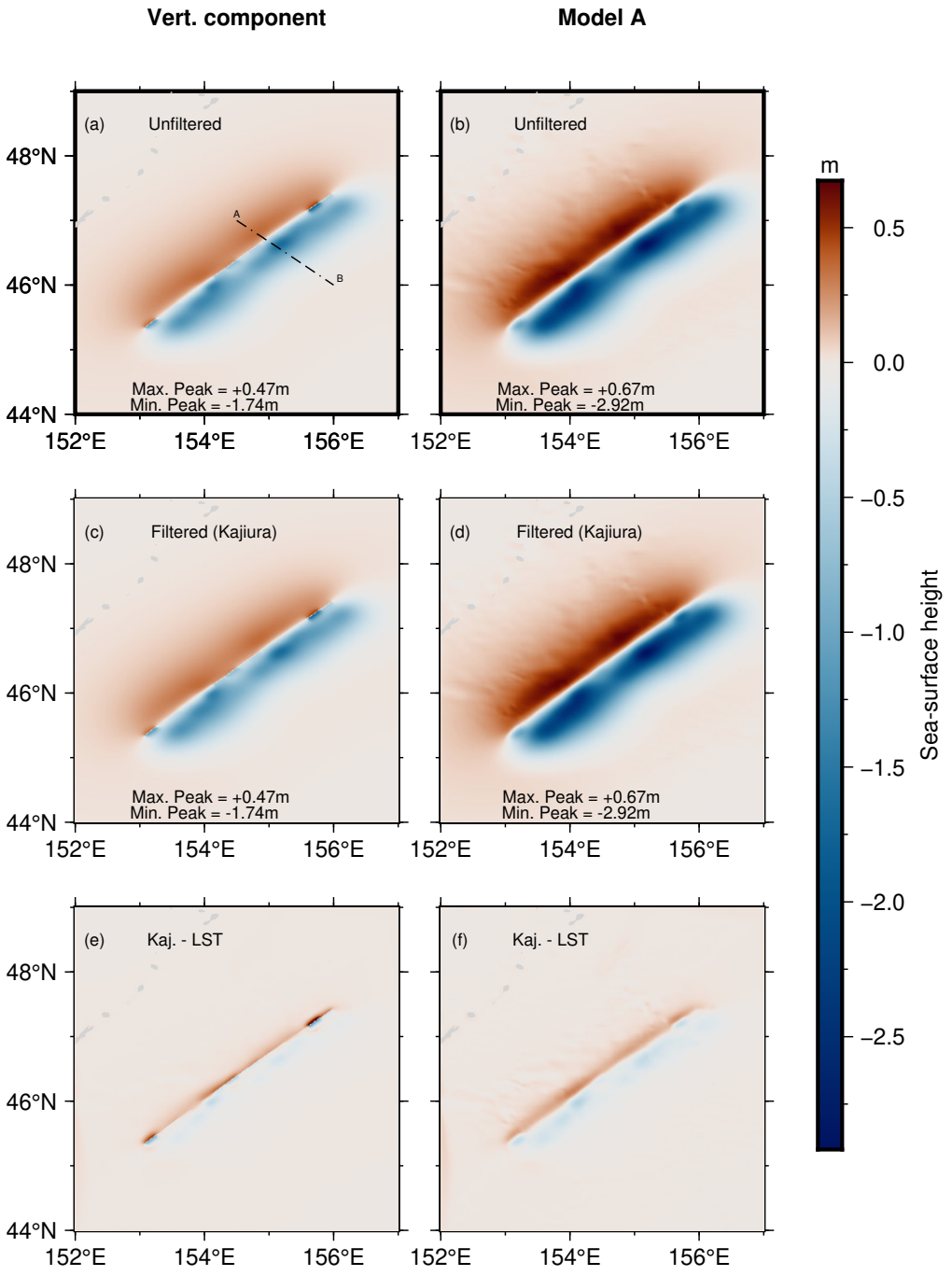

Figure S13. Results for the tsunamigenic earthquake occurred on January 13, 2007. The fault plane is southeast dipping. Panel (a) depicts the transect AB where 1D profiles for all models have been considered. Panels (e) and (f) show the spatial distributions of the simple differences between the initial conditions obtained by the application of the Kajiura-type filter and LST.

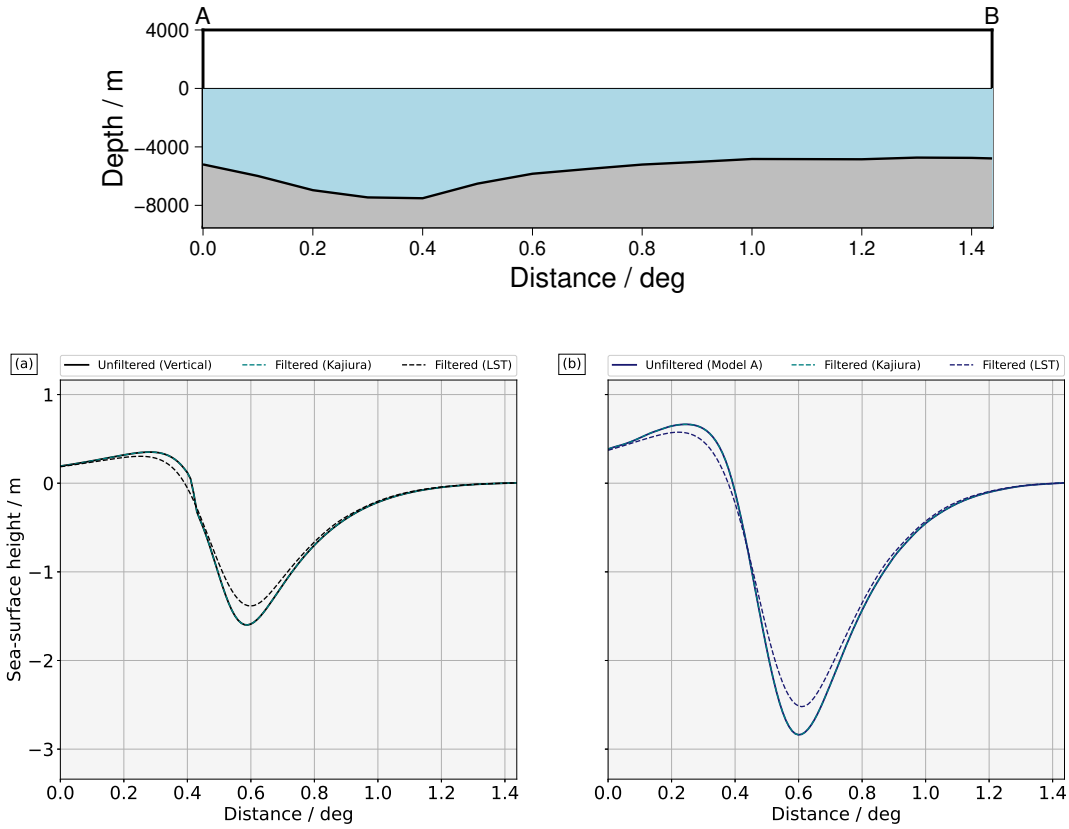

Figure S14. The picture refers the 2007 event in case of a source oriented to the southeast. The transect considered is the one depicted in Fig. S13a. Similarly to the Fig. S12, The upper panel illustrates the bathymetric profile along it. (a) The profiles are taken from the initial conditions in Figure S11 (a, c, e), considering only the vertical component. (b) The profiles are taken from the initial conditions in Figure S11 (b, d, f), considering the effect of the horizontal component through Model A.

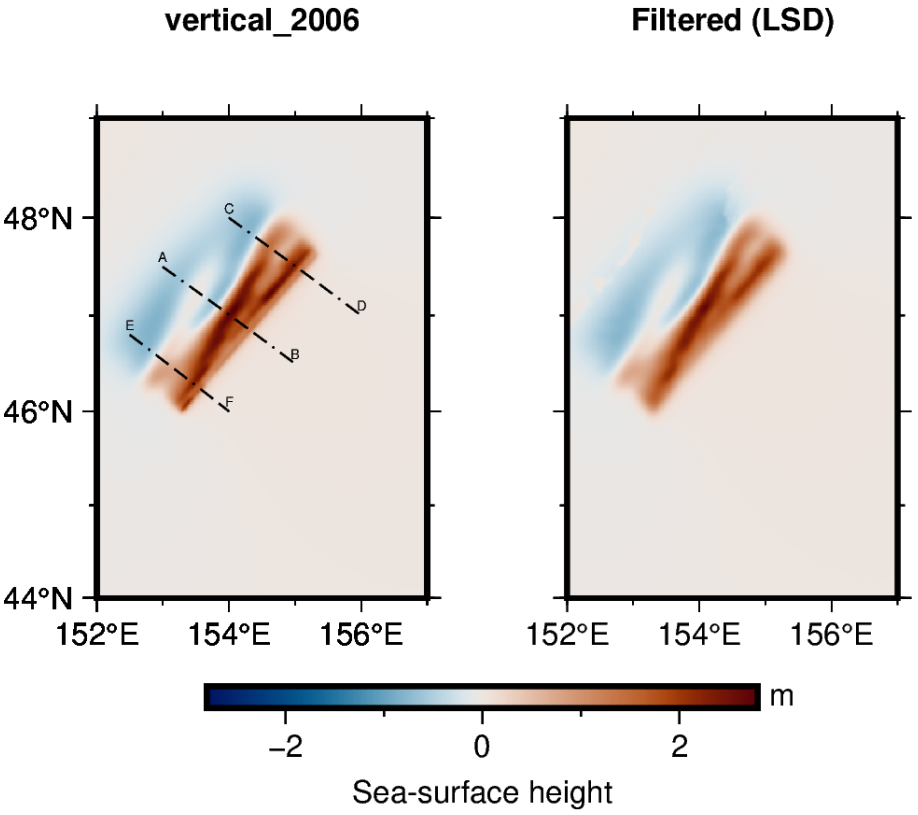

(a) Transects along the sea-surface height distribution resulting from the vertical component of the coseismic deformation, for the megathrust occurred in late 2006 (Central Kuril Islands).

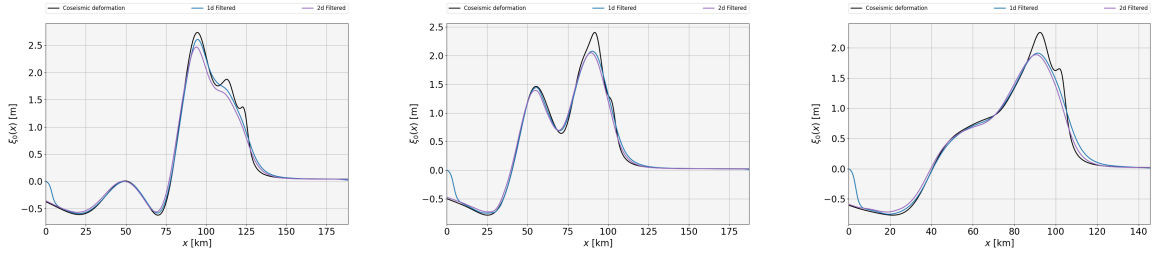

(b) Comparison of the superpositions in 1D and in 2D along the profile A-B.

(c) Comparison of the superpositions in 1D and in 2D along the profile C-D.

(d) Comparison of the superpositions in 1D and in 2D along the profile E-F.

Figure S15. Results for the 2006 event, considering a coseismic deformation resulting from the vertical component.

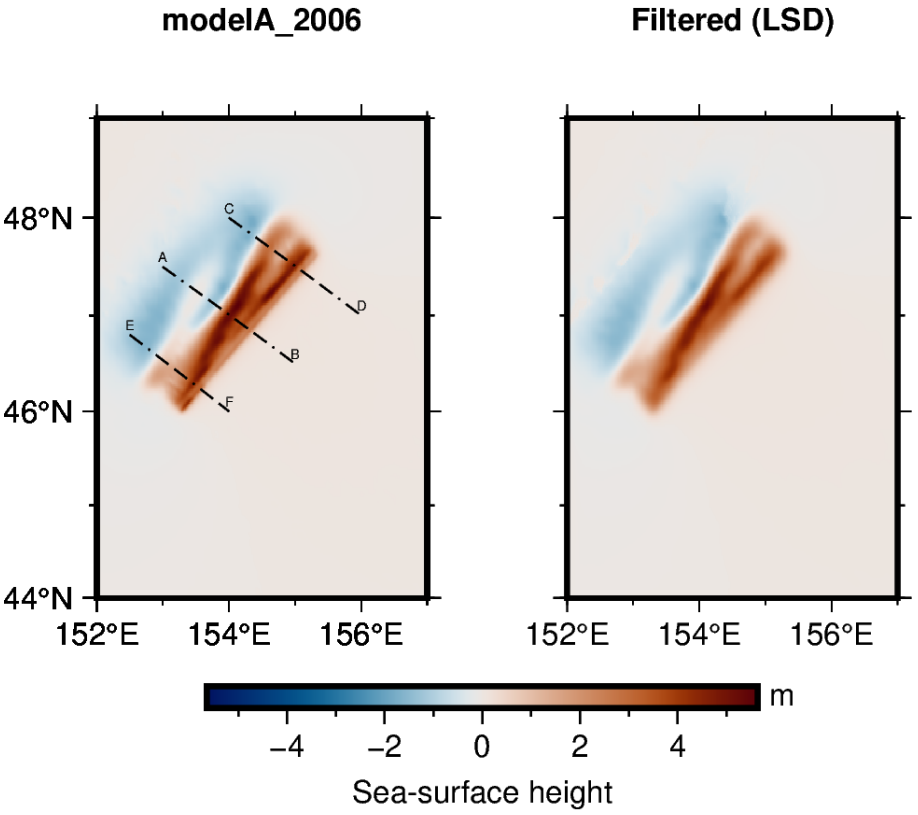

(a) Transects along the sea-surface height distribution resulting from Model A, for the megathrust occurred in late 2006 (Central Kuril Islands).

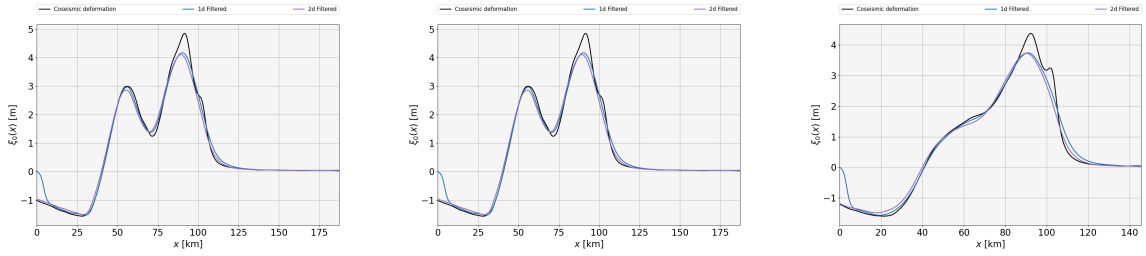

(b) Comparison of the superpositions in 1D and in 2D along the profile A-B.

(c) Comparison of the superpositions in 1D and in 2D along the profile C-D.

(d) Comparison of the superpositions in 1D and in 2D along the profile E-F.

Figure S16. Results for the 2006 event, when accounting for Model A.

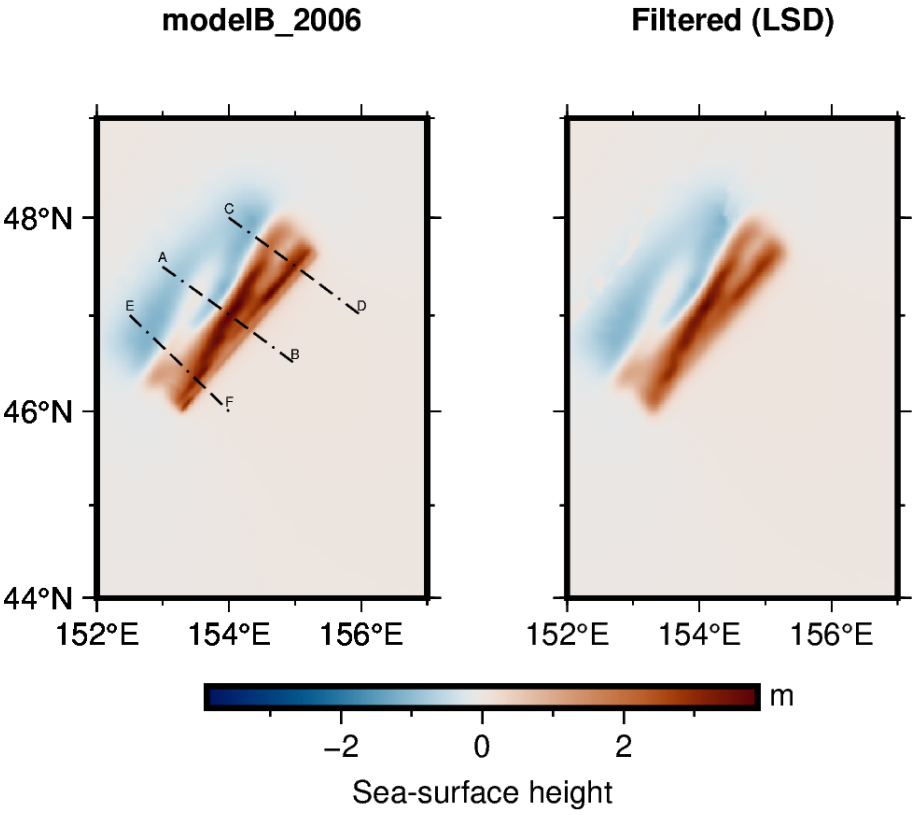

(a) Transects along the sea-surface height distribution resulting from Model B, for the megathrust occurred in late 2006 (Central Kuril Islands).

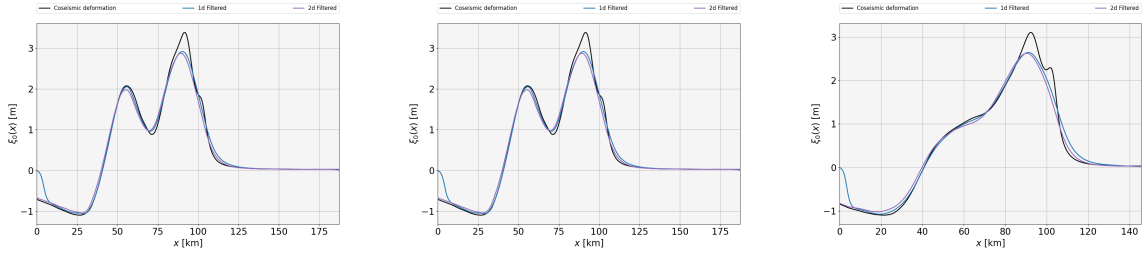

(b) Comparison of the superpositions in 1D and in 2D along the profile A-B.

(c) Comparison of the superpositions in 1D and in 2D along the profile C-D.

(d) Comparison of the superpositions in 1D and in 2D along the profile E-F.

Figure S17. Results for the 2006 event, when accounting for Model B.

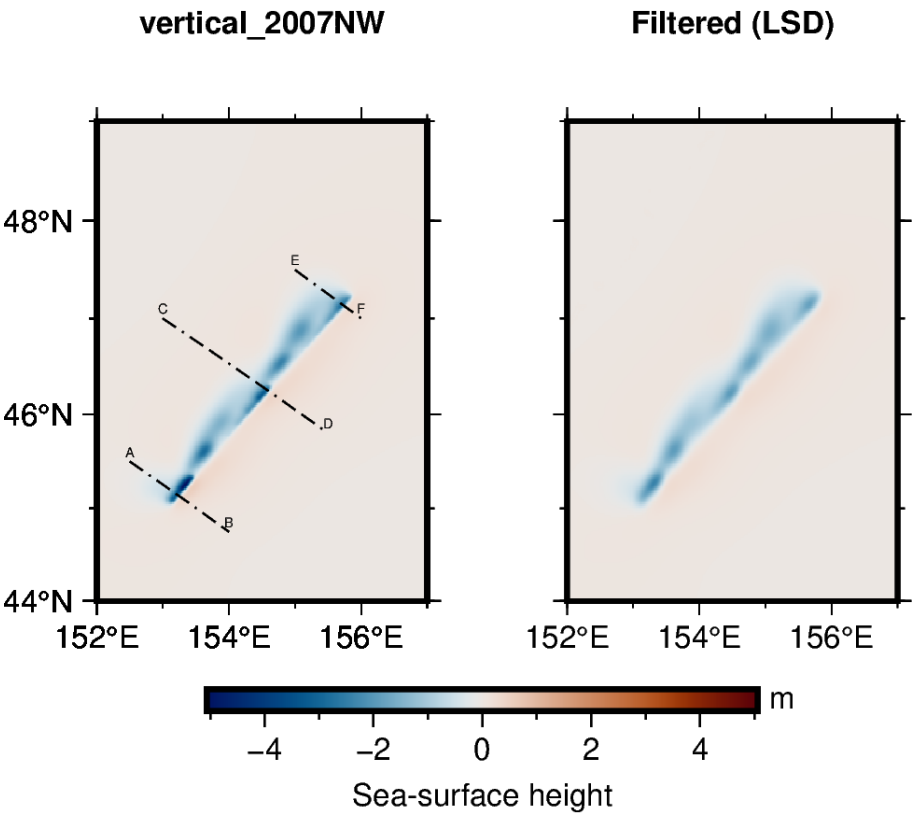

(a) Transects along the sea-surface height distribution resulting from the vertical component of the coseismic deformation, for the outer-rise occurred in early 2007, with north-west dipping (Central Kuril Islands).

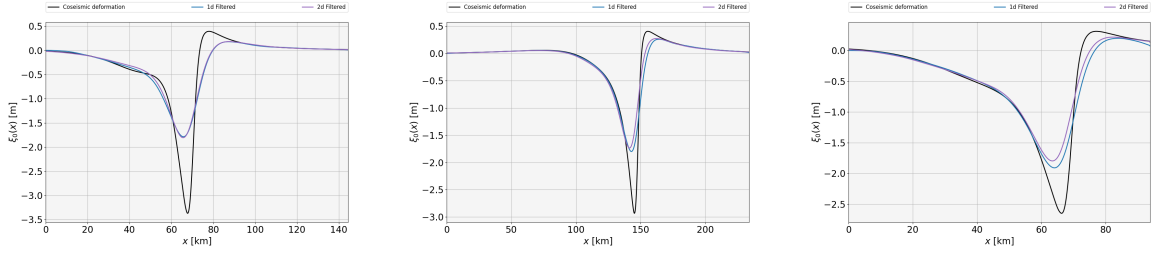

(b) Comparison of the superpositions in 1D and in 2D along the profile A-B.

(c) Comparison of the superpositions in 1D and in 2D along the profile C-D.

(d) Comparison of the superpositions in 1D and in 2D along the profile E-F.

Figure S18. Results for the 2007 event, considering a coseismic deformation resulting from the vertical component. The source is oriented northwest (NW).

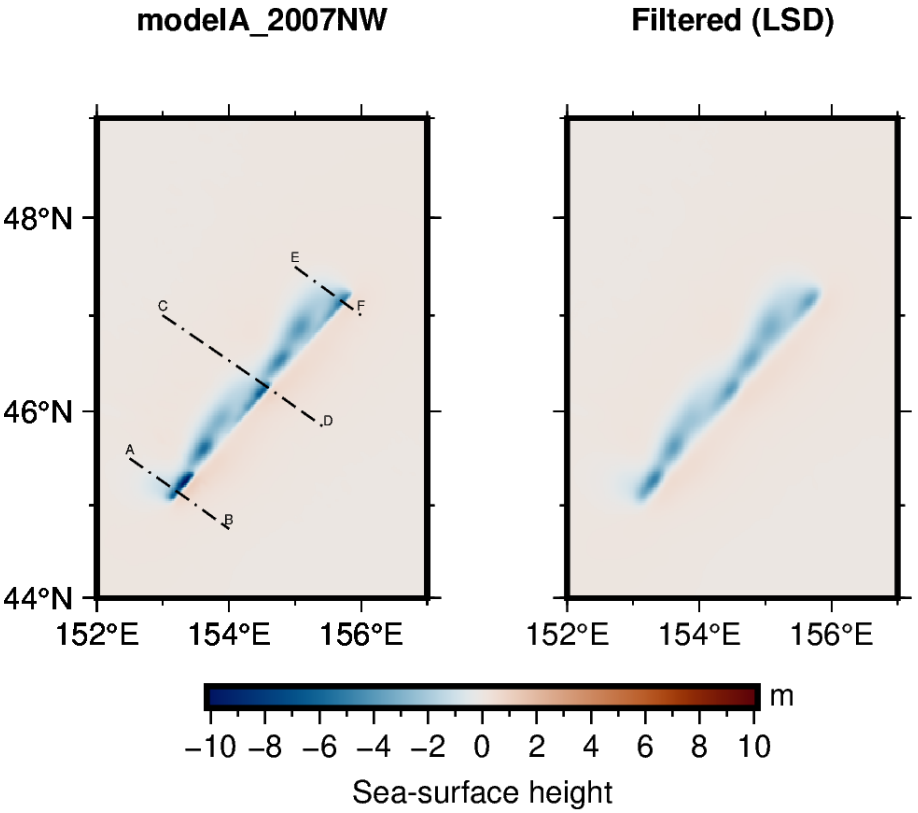

(a) Transects along the sea-surface height distribution resulting from Model A, for the outer-rise occurred in early 2007, with north-west dipping (Central Kuril Islands).

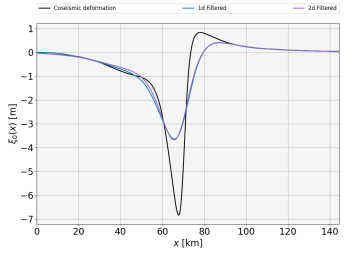

(b) Comparison of the superpositions in 1D and in 2D along the profile A-B.

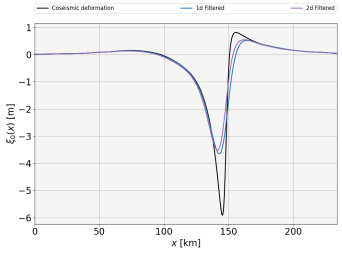

(c) Comparison of the superpositions in 1D and in 2D along the profile C-D.

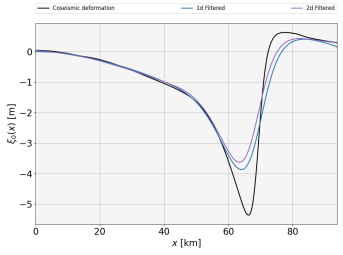

(d) Comparison of the superpositions in 1D and in 2D along the profile E-F.

Figure S19. Results for the 2007 event, when accounting for Model A. The source is oriented northwest (NW).

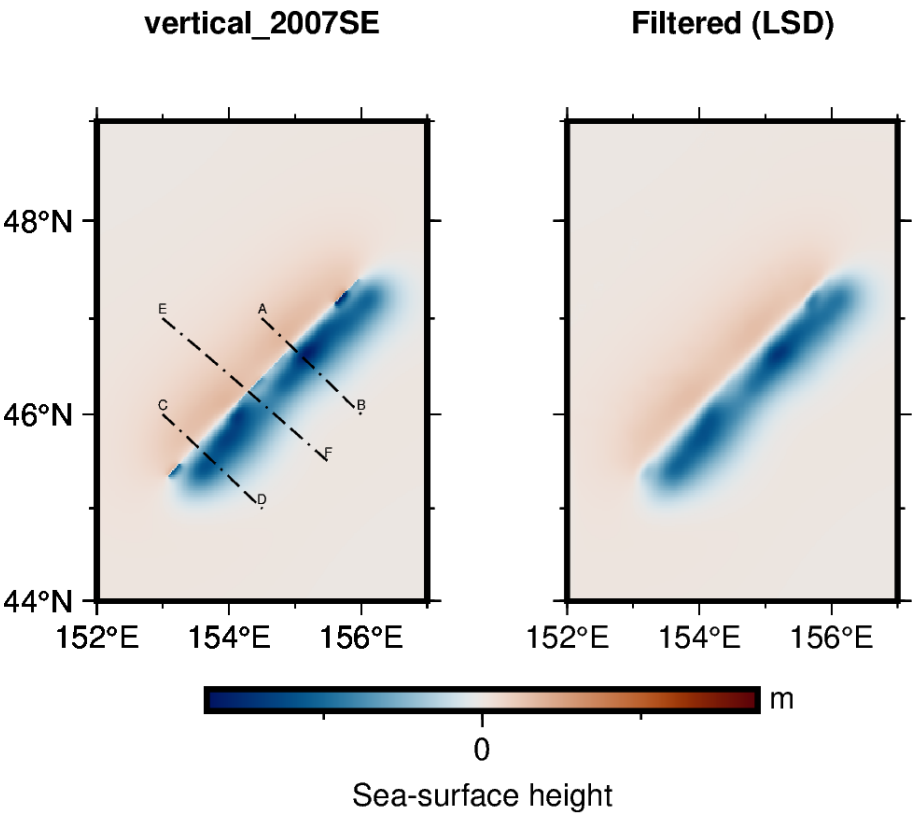

(a) Transects along the sea-surface height distribution resulting from the vertical component of the coseismic deformation, for the outer-rise occurred in early 2007, with south-east dipping (Central Kuril Islands).

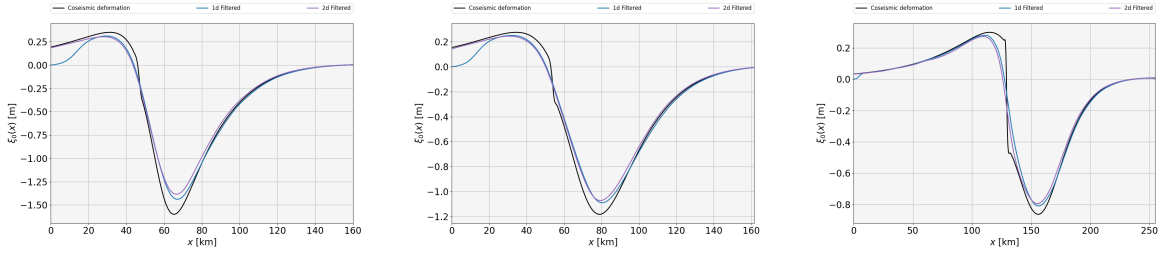

(b) Comparison of the superpositions in 1D and in 2D along the profile A-B.

(c) Comparison of the superpositions in 1D and in 2D along the profile C-D.

(d) Comparison of the superpositions in 1D and in 2D along the profile E-F.

Figure S20. Results for the 2007 event, considering a coseismic deformation resulting from the vertical component. The source is oriented southeast (SE).

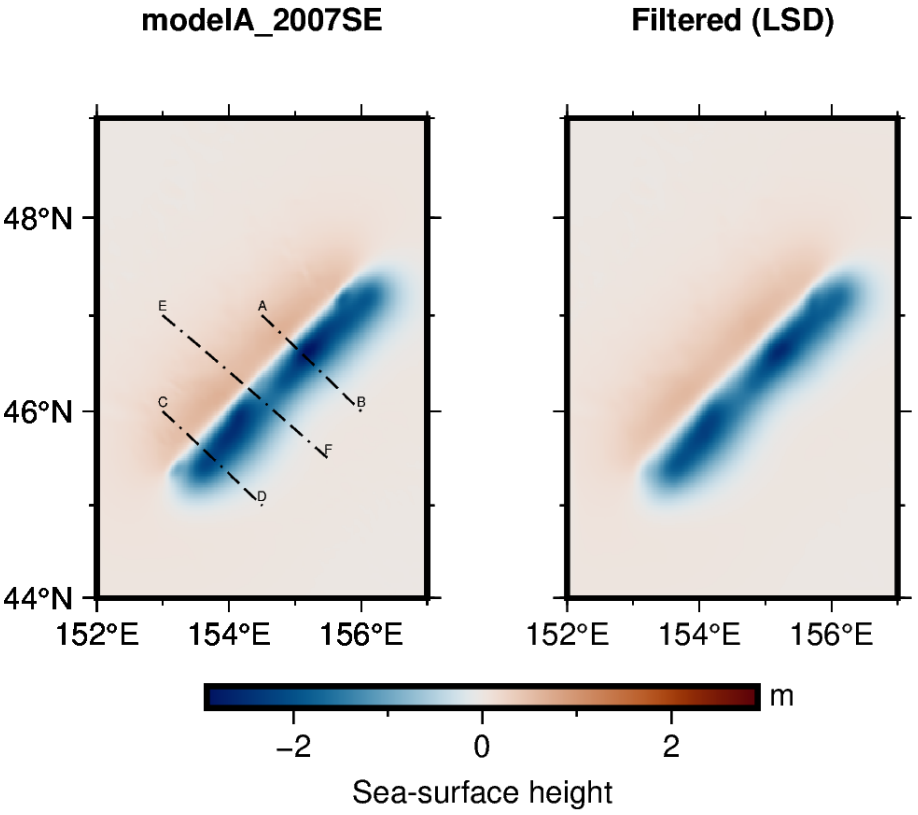

(a) Transects along the sea-surface height distribution resulting from Model A, for the outer-rise occurred in early 2007, with south-east dipping (Central Kuril Islands).

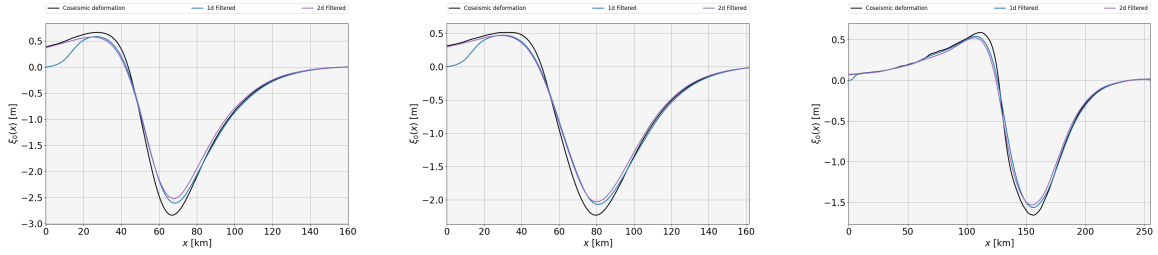

(b) Comparison of the superpositions in 1D and in 2D along the profile A-B.

(c) Comparison of the superpositions in 1D and in 2D along the profile C-D.

(d) Comparison of the superpositions in 1D and in 2D along the profile E-F.

Figure S21. Results for the 2007 event, when accounting for Model A. The source is oriented southeast (SE).

References

Filon, L. N. G.: III.—On a quadrature formula for trigonometric integrals, Proceedings of the Royal Society of Edinburgh, 49, 38–47, 1930.

Hildebrand, F. B.: Introduction to numerical analysis, New York : McGraw-Hill, 1956.

Iserles, A.: On the numerical quadrature of highly-oscillating integrals I: Fourier transforms, IMA Journal of Numerical Analysis, 24, 365–391, https://doi.org/10.1093/imanum/24.3.365, 2004.

Kajiura, K.: The leading wave of a tsunami, Bulletin of the Earthquake Research Institute, 41, 545–571, 1963.

Nosov, M. A. and Kolesov, S. V.: Optimal Initial Conditions for Simulation of Seismotectonic Tsunamis, Pure and Applied Geophysics, 168, 1223–1237, https://doi.org/10.1007/s00024-010-0226-6, 2011.

Nosov, M. A. and Sementsov, K. A.: Calculation of the initial elevation at the tsunami source using analytical solutions, Izvestiya, Atmospheric and Oceanic Physics, 50, 539–546, https://doi.org/10.1134/S0001433814050089, 2014.

Tanioka, Y. and Seno, T.: Sediment effect on tsunami generation of the 1896 Sanriku Tsunami Earthquake, Geophysical Research Letters, 28, 3389–3392, https://doi.org/https://doi.org/10.1029/2001GL013149, 2001.